Article

Cell Chemical Biology

Fatty acid chain length drives lysophosphatidylserine-dependent immunological outputs

Highlights

- Synthesis of methyl esters of lyso-PSs with varying lipid tails and their metabolism
- Very-long-chain lyso-PSs signal through TLR2 to cause neuroinflammation
- Role of long-chain lyso-PSs in macrophage signaling and mast cell degranulation
- ABHD12 is a major lyso-PS lipase in primary mast cells

Authors

Neha Khandelwal, Minhaj Shaikh, Amol Mhetre, ..., Kithiganahalli Narayanaswamy Balaji, Harinath Chakrapani, Siddhesh S. Kamat

Correspondence

amol@iiserpune.ac.in (A.M.), harinath@iiserpune.ac.in (H.C.), siddhesh@iiserpune.ac.in (S.S.K.)

In Brief

Khandelwal et al. synthesize a library of methyl esters of lysophosphatidylserines (lyso-PSs) to facilitate rigorous structure-activity relationship studies, toward understanding the role played by the lipid tail of lyso-PSs in regulating the activation of macrophages and mast cell degranulation.

Khandelwal et al., 2021, Cell Chemical Biology *28*, 1–11
June 17, 2021 © 2021 Elsevier Ltd.
https://doi.org/10.1016/j.chembiol.2021.01.008

CellPress

Please cite this article in press as: Khandelwal et al., Fatty acid chain length drives lysophosphatidylserine-dependent immunological outputs, Cell Chemical Biology (2021), https://doi.org/10.1016/j.chembiol.2021.01.008

Cell Chemical Biology

CellPress

Article

Fatty acid chain length drives lysophosphatidylserine-dependent immunological outputs

Neha Khandelwal,[1,5] Minhaj Shaikh,[2,5] Amol Mhetre,[1,5,*] Shubham Singh,[1,5] Theja Sajeevan,[1] Alaumy Joshi,[1,4] Kithiganahalli Narayanaswamy Balaji,[3] Harinath Chakrapani,[2,*] and Siddhesh S. Kamat[1,6,*]

[1]Department of Biology, Indian Institute of Science Education and Research (IISER) Pune, Dr. Homi Bhabha Road, Pashan, Pune, Maharashtra 411008, India

[2]Department of Chemistry, Indian Institute of Science Education and Research (IISER) Pune, Dr. Homi Bhabha Road, Pashan, Pune, Maharashtra 411008, India

[3]Department of Microbiology and Cell Biology, Indian Institute of Science (IISc), Bangalore, Karnataka 560012, India

[4]Present address: Department of Biochemistry & Biophysics, Texas A&M University, College Station, TX 77843, USA

[5]These authors contributed equally

[6]Lead contact

*Correspondence: amol@iiserpune.ac.in (A.M.), harinath@iiserpune.ac.in (H.C.), siddhesh@iiserpune.ac.in (S.S.K.)

https://doi.org/10.1016/j.chembiol.2021.01.008

SUMMARY

In humans, lysophosphatidylserines (lyso-PSs) are potent lipid regulators of important immunological processes. Given their structural diversity and commercial paucity, here we report the synthesis of methyl esters of lyso-PS (Me-lyso-PSs) containing medium- to very-long-chain (VLC) lipid tails. We show that Me-lyso-PSs are excellent substrates for the lyso-PS lipase ABHD12, and that these synthetic lipids are acted upon by cellular carboxylesterases to produce lyso-PSs. Next, in macrophages we demonstrate that VLC lyso-PSs orchestrate pro-inflammatory responses and in turn neuroinflammation via a Toll-like receptor 2 (TLR2)-dependent pathway. We also show that long-chain (LC) lyso-PSs robustly induce intracellular cyclic AMP production, cytosolic calcium influx, and phosphorylation of the nodal extracellular signal-regulated kinase to regulate macrophage activation via a TLR2-independent pathway. Finally, we report that LC lyso-PSs potently elicit histamine release during the mast cell degranulation process, and that ABHD12 is the major lyso-PS lipase in these immune cells.

INTRODUCTION

Lipids have long been known as potent signaling molecules that mediate many important physiological processes in mammals, including humans (Wymann and Schneiter, 2008; Dennis, 2016; Fahy et al., 2005). Prominent among the signaling lipids are the prostaglandins (Dennis and Norris, 2015), the endocannabinoids (2-arachidonoylglycerol [2-AG] and anandamide [AEA]) (Blankman and Cravatt, 2013; Fowler et al., 2005), and the well-studied lysophospholipids, sphingosine 1-phosphate (S1P) (Gonzalez-Cabrera et al., 2014; Rosen et al., 2013) and lysophosphatidic acid (lyso-PA) (Ishii et al., 2004; Contos et al., 2000). Given their physiological importance, the biosynthetic/degradative enzyme(s) and/or cognate receptor(s) of the aforementioned lysophospholipids (S1P and lyso-PA) are pharmacological targets for drugs already in clinical use or under investigation in different phases of clinical trials for an array of human neurological and immunological disorders (Gardell et al., 2006; Yanagida and Valentine, 2020). Recently, the lysophosphatidylserines (lyso-PSs) have emerged as yet another important class of signaling lysophospholipids (Shanbhag et al., 2020), with potent bioactivities in the mammalian central nervous and immune system.

Cellular pharmacological studies have shown that lyso-PSs regulate several immunological processes (Shanbhag et al., 2020) such as macrophage activation to clear apoptotic cells (Frasch and Bratton, 2012), mast cell degranulation (Lloret and Moreno, 1995), leukemic cell stimulation (Park et al., 2005), chemotaxis of human gliomas (Lee et al., 2008), and maturation of regulatory T cells (Barnes et al., 2015), and perhaps signal through Toll-like receptors (TLRs) (Van Der Kleij et al., 2002) and/or G-protein-coupled receptors (GPCRs) (Inoue et al., 2012) in the mammalian nervous and immune system. Interestingly, and of biomedical relevance, mutations to the putative lyso-PS receptors in humans have been linked to different autoimmune diseases (Szymanski et al., 2014; Napier et al., 2015; Chu et al., 2013). Murine studies have recently shown that accumulation of lyso-PS, especially very-long-chain (VLC) lyso-PSs (Blankman et al., 2013), in the mammalian brain is a major cause that drives the pathology of the early-onset human neurological disorder PHARC (polyneuropathy, hearing loss, ataxia, retinitis pigmentosa, and cataract) (Fiskerstrand et al., 2009, 2010).

Please cite this article in press as: Khandelwal et al., Fatty acid chain length drives lysophosphatidylserine-dependent immunological outputs, Cell Chemical Biology (2021), https://doi.org/10.1016/j.chembiol.2021.01.008

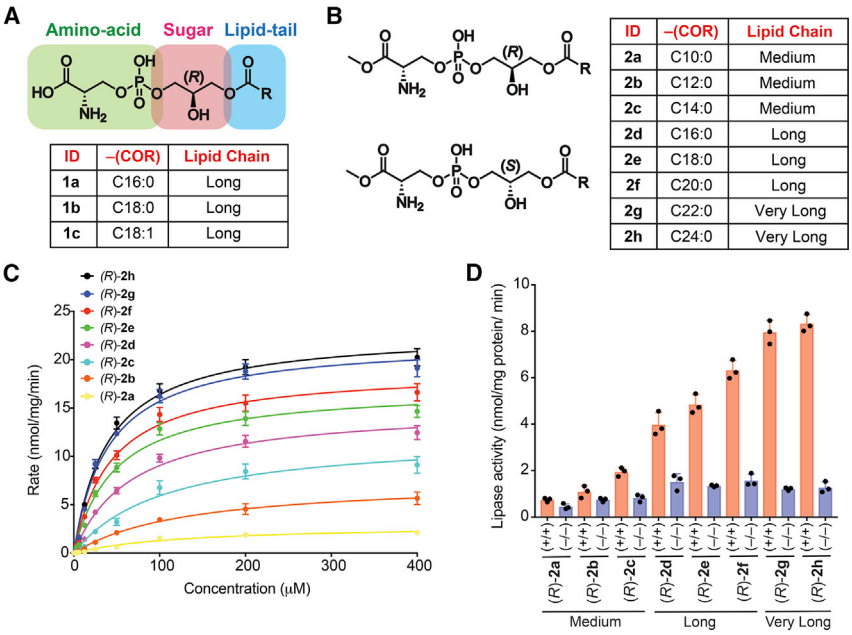

ID	–(COR)	Lipid Chain
1a	C16:0	Long
1b	C18:0	Long
1c	C18:1	Long

ID	–(COR)	Lipid Chain
2a	C10:0	Medium
2b	C12:0	Medium
2c	C14:0	Medium
2d	C16:0	Long
2e	C18:0	Long
2f	C20:0	Long
2g	C22:0	Very Long
2h	C24:0	Very Long

Figure 1. Structure of Me-lyso-PSs, and testing them as substrates against ABHD12

(A and B) The chemical structures of (A) commercially available canonical natural lyso-PSs and (B) our synthetic Me-lyso-PS lipid library with both (*R*)- and (*S*)-stereoisomers.

(C) Enzyme kinetic assays for membrane lysates (10 μg) of HEK293T cells transfected with hABHD12 tested against the (*R*)-Me-lyso-PSs (0–400 μM, 30 min, 37°C, n = 3/data point). The line connecting the points represents a fit to the Michaelis-Menten enzyme kinetics equation. See Table 1 for all enzyme kinetics parameters.

(D) Lipase assays for (*R*)-Me-lyso-PSs (100 μM, 30 min, 37°C, n = 3/group) tested against brain membrane lysates (20 μg) from wild-type (WT) (+/+) or ABHD12 knockout (−/−) mice. All data presented in (C) (data points) and (D) (bars) are presented as mean ± standard deviation (SD).

Interestingly, PHARC is caused by deleterious mutations to the *abhd12* gene (Fiskerstrand et al., 2009, 2010), which encodes an integral membrane metabolic serine hydrolase ABHD12 (α/β hydrolase domain-containing protein 12), a major and, to date, only *in vivo* functionally characterized lyso-PS lipase (Kamat et al., 2015; Blankman et al., 2013; Singh et al., 2020).

Given the strong link between lyso-PSs and human diseases, mechanistic studies are much needed to understand in more detail and biochemically characterize the signaling pathways influenced by lyso-PSs *in vivo*. Two factors complicate and/or limit such studies: (1) unlike other signaling lipids (e.g., S1P, 2-AG, AEA), *in vivo* lyso-PSs are found esterified with different fatty acids (ranging from medium-chain [C10] to VLC [C24]) (Blankman et al., 2013; Barnes et al., 2015), and hence the precise physiological contributions of the individual lyso-PSs remain cryptic; (2) commercially, lyso-PSs are limited, and even those that are available are esterified only with long-chain (LC) fatty acids (C16:0, C18:0, and C18:1) (Figure 1A). Therefore, delineating the biological contributions of medium or VLC lyso-PSs has not been possible to date.

To address the aforementioned problems, here we describe the synthesis of methyl esters of lyso-PS (Me-lyso-PS) bearing fatty acids of varying chain lengths ranging from medium-chain (C10–C14) to LC (C16–C20) to VLC (>C20) having the canonical natural (*R*)- or unnatural (*S*)-configuration at the glycerol backbone. Next, we test these synthetic Me-lyso-PS lipids in a variety of biological assays, and show that the canonical (*R*)-Me-lyso-PSs are highly bioactive while the corresponding unnatural (*S*)-Me-lyso-PSs are largely inactive. Specifically, we show that (*R*)-Me-lyso-PS are excellent substrates for the PHARC-associated lyso-PS lipase ABHD12, and confirm this enzyme's preference for VLC lyso-PS lipids (Joshi et al., 2018; Kamat et al., 2015; Blankman et al., 2013). Furthermore, we show that cellular carboxylesterases hydrolyze the methyl-ester moiety of Me-lyso-PSs to yield lyso-PSs, and thus demonstrate that the synthetic Me-lyso-PSs serve as stable prodrug-like biological precursors to lyso-PSs. Of note, we report the distinct contribution of individual lyso-PS lipids in activation and pro-inflammatory responses from macrophages and in the release of histamine during mast cell degranulation, and specifically show how the fatty acid chain length of lyso-PSs plays a critical role in the output of the aforementioned important immunological processes. Finally, we also annotate the metabolic serine hydrolase ABHD12 as a major lyso-PS lipase in primary mast cells, and expand the possible physiological role of this biomedically important lipase to an additional immunological process.

RESULTS

Synthesis of Me-lyso-PS lipids

Structurally, lyso-PSs are composed of three building blocks: (1) a sugar backbone (glycerol), (2) an amino acid head group (phospho-L-serine), and (3) a lipid tail (fatty acid) (Figure 1A) (Fahy et al., 2011). It is this intricate combination of hydrophilic (glycerol and phospho-L-serine) and hydrophobic (fatty acid) biological building blocks that confers amphiphilic properties to lyso-PSs and enables them to access different cellular membranes, organelles, and compartments. Given this amphiphilic property, lyso-PSs serve as potent hormone-like mediators of various important immunological processes (Vance, 2015; Tracey et al., 2018; Shanbhag et al., 2020). From a stereochemical perspective, all natural lyso-PSs have two chiral centers: (1) α-carbon of the phospho-L-serine head group and (2) *sn-2* carbon of the (*R*)-glycerol backbone (Figure 1A) (Mallik et al., 2018). Biosynthetically, lyso-PSs are made from phosphatidylserine (PS) precursors, by the enzymatic action of PS-specific phospholipases (Hosono et al., 2001; Kamat et al., 2015), and subsequent studies have shown that physiologically, almost all lyso-PSs exists as 1-(fatty acyl)-2-hydroxy-*sn*-glycero-3-phospho-L-serine (Iwashita et al., 2009; Kamat et al., 2015). Given the synthetic challenges in making this bioactive lipid, for example, (1) combination of the aforementioned hydrophilic and hydrophobic moieties, (2) lipophilicity of the final molecule, and (3) the need for retention in configuration of the two chiral centers toward making the correct diastereomer,

Please cite this article in press as: Khandelwal et al., Fatty acid chain length drives lysophosphatidylserine-dependent immunological outputs, Cell Chemical Biology (2021), https://doi.org/10.1016/j.chembiol.2021.01.008

Table 1. Kinetic constants for lyso-PS and Me-lyso-PS substrates tested against hABHD12 (HEK293T membrane lysates transiently transfected with hABHD12)

Lyso-PS species	Fatty acid chain length: unsaturation	V_{max} (nmol/mg protein/min)	K_M (μM)	V_{max}/K_M (nmol/mg protein/min/M) (× 10^5)
1a	16:0	15.6 ± 0.6	72 ± 8	2.2 ± 0.3
1b	18:0	18.3 ± 0.5	48 ± 4	3.8 ± 0.4
1c	18:1	17.8 ± 0.6	46 ± 6	3.8 ± 0.5
(*R*)-**2a**	10:0	2.9 ± 0.2	126 ± 18	0.2 ± 0.04
(*R*)-**2b**	12:0	7.6 ± 0.3	131 ± 14	0.6 ± 0.06
(*R*)-**2c**	14:0	12.2 ± 0.6	106 ± 14	1.1 ± 0.1
(*R*)-**2d**	16:0	15.2 ± 0.6	67 ± 7	2.3 ± 0.3
(*R*)-**2e**	18:0	17.2 ± 0.6	47 ± 5	3.7 ± 0.5
(*R*)-**2f**	20:0	19.0 ± 0.6	43 ± 4	4.4 ± 0.5
(*R*)-**2g**	22:0	22.0 ± 0.6	40 ± 4	5.5 ± 0.6
(*R*)-**2h**	24:0	22.9 ± 0.6	40 ± 4	5.7 ± 0.6
(*S*)-**2a**	10:0	0.2 ± 0.02	275 ± 32	0.007 ± 0.001
(*S*)-**2b**	12:0	0.4 ± 0.05	255 ± 35	0.016 ± 0.002
(*S*)-**2c**	14:0	0.6 ± 0.1	215 ± 28	0.028 ± 0.003
(*S*)-**2d**	16:0	0.8 ± 0.1	187 ± 24	0.043 ± 0.006
(*S*)-**2e**	18:0	1.2 ± 0.1	178 ± 25	0.067 ± 0.008
(*S*)-**2f**	20:0	1.3 ± 0.2	165 ± 23	0.078 ± 0.009
(*S*)-**2g**	22:0	1.2 ± 0.2	167 ± 26	0.072 ± 0.009
(*S*)-**2h**	24:0	1.2 ± 0.3	176 ± 31	0.068 ± 0.008

only three naturally occurring LC lyso-PSs (**1a–1c**) are commercially available, thus limiting any rigorous structure-activity relationship (SAR) studies for this important lysophospholipid class (Figure 1A). Since the commercial paucity of lyso-PSs would impede our proposed studies, here we describe a facile synthesis route toward making Me-lyso-PS esterified with saturated fatty acids of varying chain lengths ranging from medium-chain to VLC (Figure 1B and Data S1). Speculating that the free reactive carboxylate moiety of the amino acid end of the molecule might cross-react and complicate the synthesis, we decided to make the Me-lyso-PS version. Our synthetic route successfully afforded the naturally occurring canonical (*R*)-Me-lyso-PSs (Figure 1B and Data S1) and the unnatural (*S*)-Me-lyso-PSs (Figure 1B and Data S1) with the same fatty acids (Figure 1B) to yield final compounds ((*R*)-**2a–2h** or (*S*)-**2a–2h**) in milligram quantities.

ABHD12 prefers VLC lyso-PSs as substrates

The lipids previously tested as substrates for the mammalian lyso-PS lipase ABHD12 have been commercially available LC lyso-PSs (**1a–1c**) (Blankman et al., 2013; Kamat et al., 2015) (Figure 1A) and various monoacylglycerol (MAG) lipids (Blankman et al., 2007; Joshi et al., 2018; Navia-Paldanius et al., 2012). In the absence of a commercial source for medium or VLC lyso-PSs, which to the best of our knowledge have not been tested against ABHD12, the MAG lipids have served as excellent surrogates for performing SAR studies toward biochemically understanding the substrate preference for this lipase (Joshi et al., 2018). Therefore, having synthesized the library of (*R*)- and (*S*)-Me-lyso-PSs containing medium-chain, LC, and VLC variants (nomenclature in Figure 1B), we first wanted to test whether these lipids were indeed substrates for ABHD12. Leveraging established liquid chromatography coupled with mass spectrometry (LC-MS)-based substrate assays (Joshi et al., 2018), we found that both recombinant human ABHD12 (hABHD12) (Table 1 and Figure S1A) and endogenous mouse brain ABHD12 (mABHD12) (Figure S1B) robustly turned over (*R*)-Me-lyso-PSs, and for the same fatty acid, LC (*R*)-Me-lyso-PS and corresponding canonical natural LC lyso-PS behaved almost identically. Next, we performed rigorous enzyme kinetics measurements for our (*R*)-Me-lyso-PS library against hABHD12 (Figure 1C and Table 1) and found that hABHD12 strongly prefers VLC (*R*)-Me-lyso-PSs as substrates, with (*R*)-**2h** (C24:0, V_{max} = 22.9 ± 0.6 nmol/mg protein/min, K_M = 40 ± 4 μM) and (*R*)-**2g** (C22:0, V_{max} = 22.0 ± 0.6 nmol/mg protein/min, K_M = 40 ± 4 μM) being the best substrates. Furthermore, mouse brain membrane lysates were assayed against the same Me-lyso-PS library, and here too we found that mABHD12 strongly prefers VLC (*R*)-Me-lyso-PSs, with (*R*)-**2h** (C24:0, rate = 8.2 ± 0.3 nmol/mg protein/min) and (*R*)-**2g** (C22:0, rate = 8.0 ± 0.3 nmol/mg protein/min) being the best substrates (Figure 1D). In this experiment, mouse brain membrane lysates from ABHD12-null mice were used as controls to delineate specific contributions from mABHD12 (Figure 1D). In both these assays, we also tested (*S*)-Me-lyso-PSs and found, not surprisingly, that these were very poor substrates for hABHD12 (Table 1 and Figure S1C) and mABHD12 (Figure S1D), with catalytic efficiencies 100-fold lower than that of corresponding (*R*)-Me-lyso-PSs for hABHD12 (Table 1). Taken together, these substrate assays conclusively show that the ABHD12-catalyzed lyso-PS lipase reaction is highly stereospecific, prefers VLC (*R*)-lyso-PSs as substrates, and, together with recent findings (Singh et al., 2020; Joshi et al., 2018), now provides a concrete biochemical explanation as to why VLC lyso-PSs accumulate the most in ABHD12 knockout mouse brains (Blankman et al., 2013).

Please cite this article in press as: Khandelwal et al., Fatty acid chain length drives lysophosphatidylserine-dependent immunological outputs, Cell Chemical Biology (2021), https://doi.org/10.1016/j.chembiol.2021.01.008

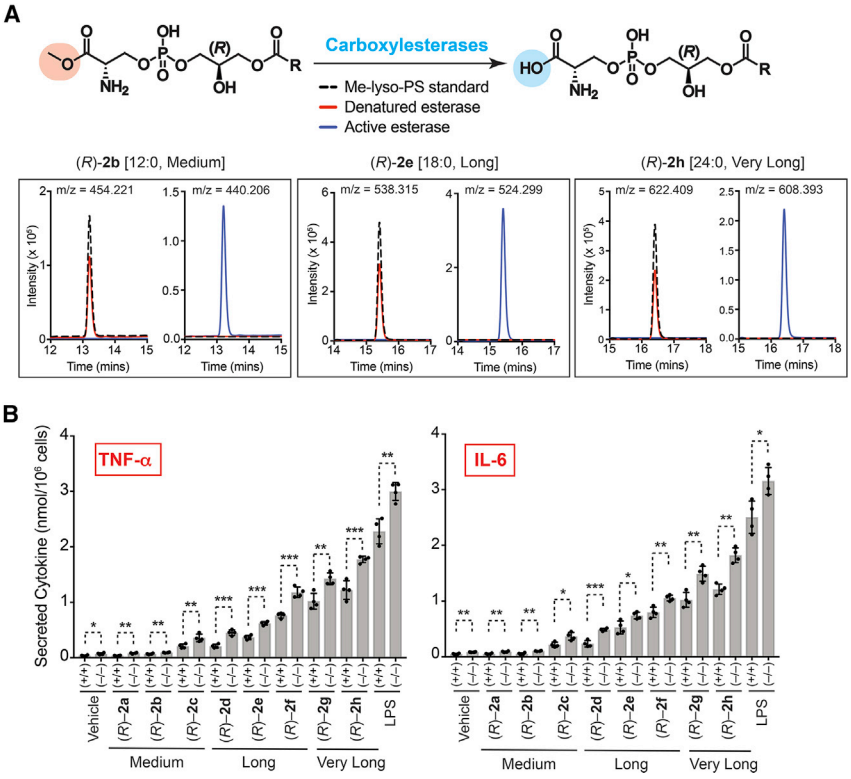

Figure 2. Metabolism of Me-lyso-PSs by carboxylesterases and the pro-inflammatory activity of Me-lyso-PSs in macrophages

(A) Top: the enzymatic reaction for metabolism (hydrolysis) of Me-lyso-PSs to the corresponding lyso-PSs catalyzed by carboxylesterases. Bottom: extracted ion chromatograms from a LC-MS analysis of (*R*)-**2b** (C12:0) ($[M-H]^-$ = 454.221), (*R*)-**2e** (C18:0) ($[M-H]^-$ = 538.315), and (*R*)-**2h** (C24:0) ($[M-H]^-$ = 622.409) showing the complete conversion of the parent compound (Me-lyso-PS) to the corresponding lyso-PS (loss of 14 Da) following treatment with active (blue trace), but not denatured (red trace), porcine liver carboxylesterase (0.1 U, 15 min, 37°C). In these assays, 100 μg of the (*R*)-Me-lyso-PS was used, and a no-enzyme standard only control (dotted black trace) was also included for the same treatment. This LC-MS experiment was done twice for each of the (*R*)-Me-lyso-PS, with reproducible results each time.

(B) Secreted TNF-α and IL-6 from PPMs harvested from WT (+/+) or ABHD12 knockout (−/−) mice following treatment with vehicle (DMSO) or lipopolysaccharide (LPS) or (*R*)-**2a–2h** (1 μM, 4 h, 37°C); All data are presented as mean ± SD (n = 4/group). *p < 0.05, **p < 0.01, ***p < 0.001 versus (+/+) group by Student's two-tailed unpaired parametric t test.

Cellular carboxylesterases metabolize Me-lyso-PS to lyso-PS

Having synthesized Me-lyso-PSs, we postulated that these might be metabolized by cellular carboxylesterases to yield the corresponding lyso-PSs (Figure 2A). To test this hypothesis, we incubated three (*R*)-Me-lyso-PSs of varying lipid tails ((*R*)-**2b** [C12:0, medium-chain], (*R*)-**2e** [C18:0, LC], or (*R*)-**2b** [C24:0, VLC]) with active or denatured porcine liver carboxylesterase, and upon this treatment, by LC-MS (Joshi et al., 2018) we checked for the formation of the corresponding canonical lyso-PSs. We found for all the three (*R*)-Me-lyso-PSs subjected to this treatment that upon incubation with active but not the denatured carboxylesterase, the (*R*)-Me-lyso-PS was completely consumed and a new peak was observed with mass shift of ∼14 Da (parent *m/z* − 14 Da) (Figure 2A). The mass of this new peak corresponds to the loss of the methyl group from (*R*)-Me-lyso-PS to yield the corresponding canonical (*R*)-lyso-PS via hydrolysis by the carboxylesterase (Figure 2A). Since we planned to test this synthetic Me-lyso-PS library for different biological activities in mammalian macrophages and mast cells, we decided to test whether lysates of these immune cells had carboxylesterases capable of converting (*R*)-Me-lyso-PSs to the canonical lyso-PSs. To negate any lyso-PS lipase type activity, we used active or denatured lysates from ABHD12-null primary peritoneal macrophages or peritoneal-derived cultured mast cells, and found that the active but not denatured lysates from both these immune cells converted the three previously tested (*R*)-Me-lyso-PSs, namely, (*R*)-**2b** (C12:0, medium-chain), (*R*)-**2e** (C18:0, LC), and (*R*)-**2h** (C24:0, VLC), to their corresponding canonical (*R*)-lyso-PS lipid (Figure S2A). Our results clearly show that cellular carboxylesterases can hydrolyze the methyl group of (*R*)-Me-lyso-PSs to yield the corresponding canonical (*R*)-lyso-PSs (Figure 2A) and that the synthetic Me-lyso-PSs serve as stable prodrug-like biological surrogates to lyso-PSs, making them amenable to testing in primary macrophages and mast cells.

VLC lyso-PSs elicit robust pro-inflammatory responses in mammalian macrophages

Lyso-PSs have previously been shown to elicit immunological responses via pro-inflammatory cytokine secretion (e.g., tumor necrosis factor α [TNF-α], interleukin-6 [IL-6]) from mammalian macrophages (Kamat et al., 2015; Frasch and Bratton, 2012), and we wanted to assess whether the Me-lyso-PSs were capable of the same, having shown that carboxylesterases in primary macrophages can metabolize Me-lyso-PSs to lyso-PSs (Figure S2A). We found that when primary peritoneal macrophages (PPMs) isolated from wild-type (WT) mice were treated with equal concentrations of the canonical LC lyso-PSs (**1a** [C16:0] and **1b** [C18:0]) and the corresponding (*R*)-Me-lyso-PSs ((*R*)-**2d** and (*R*)-**2e**) of the same lipid tail, they secreted almost equal amounts of pro-inflammatory cytokines (TNF-α, IL-6) (Figure S2B). Not surprisingly, treating PPMs with unnatural (*S*)-Me-lyso-PSs (Figure S2C), corresponding free fatty acids (Figure S2C), or other lysophospholipids (lysophosphatidic acid [lyso-PA], lysophosphatidylglycerol [lyso-PG], and lysophosphatidylcholine [lyso-PC]) with same lipid tail (Figure S2D) failed to elicit any inflammatory response, suggesting that ligand recognition in PPMs in eliciting pro-inflammatory responses is highly stereospecific for (*R*)-lyso-PSs. Having established comparable bioactivities of canonical lyso-PSs and (*R*)-Me-lyso-PSs, we isolated PPMs from WT or ABHD12

Please cite this article in press as: Khandelwal et al., Fatty acid chain length drives lysophosphatidylserine-dependent immunological outputs, Cell Chemical Biology (2021), https://doi.org/10.1016/j.chembiol.2021.01.008

CellPress

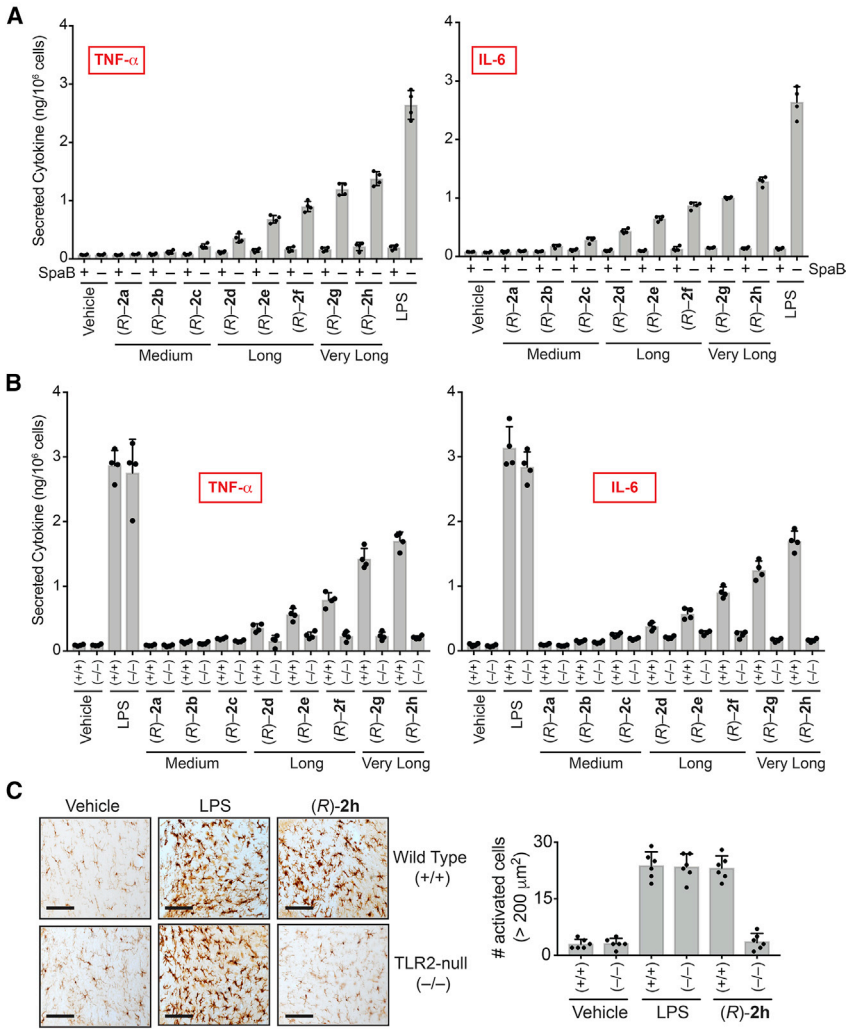

Figure 3. VLC lyso-PSs elicit pro-inflammatory responses via a TLR2-dependent pathway

(A and B) Secreted TNF-α and IL-6 from PPMs harvested from: (A) WT mice pre-treated with DMSO or SpaB (10 μM, 4 h, 37°C), followed by treatment with vehicle or LPS or (*R*)-**2a–2h** (1 μM, 4 h, 37°C); (B) WT (+/+) or TLR2 knockout (−/−) mice following treatment with vehicle or LPS or (*R*)-**2a–2h** (1 μM, 4 h, 37°C).

(C) Representative images from Iba-1 immunostaining for microglial activation (scale bars, 250 μm) and quantification of enlarged cells (>200 μm^2) in the cerebellum (per 1.44 mm^2) of WT (+/+) or TLR2 knockout (−/−) mice following intravenous injection of vehicle (PBS), LPS, or (*R*)-**2h** (C24:0) (all 1 mg/kg body weight, 10 h).

All data are presented as mean ± SD (n = 4–6/group).

knockout mice and incubated them with the (*R*)-Me-lyso-PS library to determine whether the length of lipid tail had any effect on pro-inflammatory cytokine secretion. Interestingly, we found from this SAR study that VLC (*R*)-Me-lyso-PSs, particularly (*R*)-**2g** (C22:0) and (*R*)-**2h** (C24:0), produced the highest pro-inflammatory cytokine secretion (TNF-α, IL-6) from WT PPMs (Figure 2B). Not surprisingly, ABHD12-null PPMs secreted significantly more pro-inflammatory cytokines compared with WT PPMs upon (*R*)-Me-lyso-PS treatments, consistent with their diminished lyso-PS lipase activity (Kamat et al., 2015) (Figure 2B). For either genotype, the pharmacological Me-lyso-PS treatments did not have any effect on cell viability.

Here, we used the bacterial outer membrane glycolipid lipopolysaccharide (LPS) as a positive control, as this endotoxin tested in PPMs mimics Gram-negative bacteria and robustly elicits immunological responses (pro-inflammatory cytokine secretion) in PPMs toward clearing this infection via a TLR4-dependent pathway (Raetz and Whitfield, 2002). In these assays, we found that the VLC (*R*)-Me-lyso-PS treatments produced ~60% pro-inflammatory cytokine secretion relative to similar LPS treatments in PPMs, suggesting that like LPS, VLC (*R*)-Me-lyso-PSs are potent immunological activators in mammalian macrophages (Figure 2B). We also performed a similar SAR study in human THP-1 macrophages and found similar results whereby VLC (*R*)-Me-lyso-PSs produced the highest secretion of pro-inflammatory cytokines (Figure S2E).

VLC lyso-PSs signal via TLR2 in mammalian macrophages

Reported literature speculates that VLC lyso-PSs perhaps signal through TLR2 (Van Der Kleij et al., 2002) although, to the best of our knowledge, VLC lyso-PSs have never been directly tested against any receptor for any immunological activity given their commercial unavailability. We found from a large-scale gene expression database (Figure S3A) (Wu et al., 2016) and by RT-PCR analysis (Figure S3B) that TLR2 (but none of the other putative lyso-PS receptors [Inoue et al., 2012]) is enriched on WT PPMs. Next, we found that pharmacological antagonism of TLR2 using Sparstolonin B (SpaB) (Liang et al., 2011) ablated the increased pro-inflammatory cytokine secretion caused by VLC (*R*)-Me-lyso-PS treatments in WT PPMs (Figure 3A), and in human THP-1 macrophages (Figure S2F). Here, we found that SpaB treatment also ablated the increased pro-inflammatory cytokine secretion caused by LPS treatment in WT PPMs (Figure 3A), consistent with SpaB's dual TLR2/TLR4 antagonism activity (Liang et al., 2011, 2013). Furthermore, we harvested PPMs from TLR2 knockout mice (Figure S3C) (Holla et al., 2016) and measured pro-inflammatory cytokine secretion following (*R*)-Me-lyso-PS treatments. Consistent with the pharmacological studies, we found that VLC (*R*)-Me-lyso-PSs, particularly (*R*)-**2g** and (*R*)-**2h**, produced highest secretion of TNF-α and IL-6 from WT PPMs, and this pro-inflammatory cytokine secretion was almost absent in TLR2-null PPMs (Figure 3B).

ABHD12 knockout mice display increased cerebellar microgliosis, whereby the accumulation of VLC lyso-PSs speculatively causes this neuroinflammatory phenotype (Blankman et al., 2013). To test whether VLC lyso-PSs indeed causes

Please cite this article in press as: Khandelwal et al., Fatty acid chain length drives lysophosphatidylserine-dependent immunological outputs, Cell Chemical Biology (2021), https://doi.org/10.1016/j.chembiol.2021.01.008

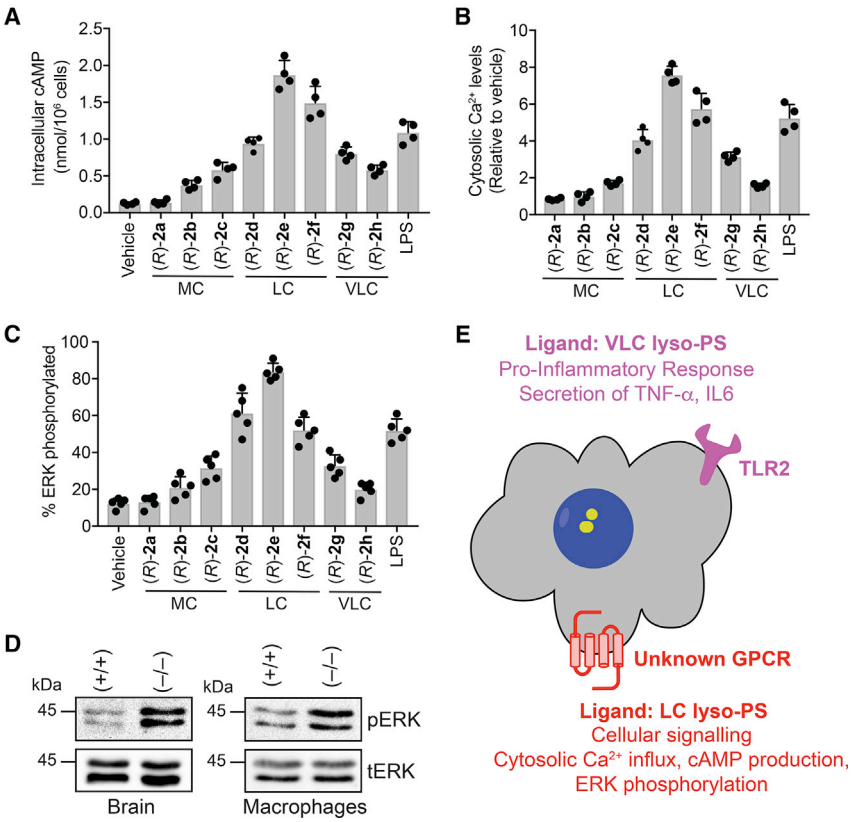

Figure 4. LC lyso-PSs activate macrophages through a putative GPCR

(A–C) (A) Intracellular cAMP, (B) relative cytosolic Ca^{2+} levels, and (C) percentage of phosphorylated ERK from WT PPMs following treatment with vehicle (DMSO) or LPS or (*R*)-**2a–2h** (1 μM, 10 min, 37°C). All data are presented as mean ± SD (n = 4–5/group), where MC denotes medium chain, LC long chain, and VLC very long chain.

(D) Representative western blots on lysates from brains (6-month-old mice) and LPS-treated (1 μM, 4 h, 37°C) PPMs harvested from WT (+/+) or ABHD12-null (−/−) mice, showing enhanced phosphorylation of ERK in both these tissues for the ABHD12-null (−/−) genotype.

(E) Schematic representation summarizing the lyso-PS signaling pathways by possibly two types of receptors on mammalian macrophages.

neuroinflammation and if they signal through TLR2, we intravenously injected a VLC (*R*)-Me-lyso-PS ((*R*)-**2h**, C24:0) into WT or TLR2-null mice, and quantified the extent of neuroinflammation by counting the number of activated microglia using an established immunohistochemical protocol (Singh et al., 2020; Blankman et al., 2013). We found that systemic administration of (*R*)-**2h** (C24:0) robustly induced cerebellar microgliosis in WT but not TLR2 knockout mice, suggesting that VLC (*R*)-Me-lyso-PSs signals through TLR2, causing neuroinflammation (Figures 3C and S4). As a positive control, we used LPS (which signals through TLR4) (Raetz and Whitfield, 2002) and intravenously injected it at the same dose and time, and found that the extent of neuroinflammation in WT and TLR2-null mice was almost identical (Figures 3C and S4). Furthermore, we found that relative to the positive control LPS, the VLC (*R*)-Me-lyso-PS (*R*)-**2h** (C24:0) produced comparable neuroinflammation (Figures 3C and S4). Interestingly, a LC (*R*)-Me-lyso-PS ((*R*)-**2e**, C18:0) intravenous injection for the same dosing regimen did not produce any neuroinflammation in WT mice (Figures S4A and S4B). Taken together, our results provide compelling *in vivo* evidence that VLC lyso-PSs (but not LC lyso-PSs) signal through TLR2, elicit a robust pro-inflammatory immune response, and are likely responsible for the neuroinflammation observed in ageing ABHD12 knockout mice, the murine model of PHARC (Blankman et al., 2013).

Mammalian macrophages have a cryptic lyso-PS receptor

Mammalian macrophages in response to lyso-PS produce increased intracellular cyclic adenosine 5′-monophosphate (cAMP) (Sugita et al., 2013), cytosolic calcium (Ca^{2+}) influx (Park et al., 2005), and heightened phosphorylation of the nodal extracellular signal-regulated kinase (ERK) (Lee et al., 2008; Sugita et al., 2013), and we wanted to test whether Me-lyso-PSs also produce these phenotypes in mammalian macrophages. We found in WT PPMs that cellular cAMP (Figure 4A), relative cytosolic Ca^{2+} levels (Figure 4B), and ERK phosphorylation (Figure 4C) increased most profoundly upon treatment with LC (*R*)-Me-lyso-PSs, especially (*R*)-**2e** (C18:0), and that medium-chain or VLC (*R*)-Me-lyso-PS had negligible effects on these phenotypes. Surprisingly, the genetic deletion of TLR2 in PPMs (Figures S5A, S5B, and S6C) or its pharmacological antagonism in PPMs (Figures S5C, S5D, and S6B) and human THP-1 macrophages (Figures S5E, S5F, and S6B) showed no change on any of these phenotypes following (*R*)-Me-lyso-PS treatment. We also found that the LC (*R*)-Me-lyso-PSs (*R*)-**2e** (C18:0) and the corresponding canonical lyso-PS **1b** (C18:0) behaved identically in all these assays (Figures S6D–S6F). Not surprisingly, upon treating PPMs with (*S*)-Me-lyso-PSs (Figures S6A, S6E, and S6F), the corresponding free fatty acids or other lysophospholipids with lipid tail (C18:0) (Figures S6D–S6F), failed to elicit any significant response in any of these assays under similar treatment conditions, suggesting that these phenotypes in mammalian macrophages are specific to LC (*R*)-Me-lyso-PS (particularly C18:0). In all these assays, we found that the pharmacological Me-lyso-PS treatments did not affect cell viability.

Of note, brains and LPS-treated PPMs derived from ABHD12-null mice (where, in absolute concentrations, **1b** [C18:0 lyso-PS] is the most abundant, and significantly deregulated lyso-PS [Blankman et al., 2013; Kamat et al., 2015]) have markedly more ERK phosphorylation compared with WT control (Figure 4D). Given the heightened intracellular cAMP, cytosolic Ca^{2+} influx, phosphorylation of ERK, and inability of pharmacological antagonism or genetic disruption of TLR2 to affect any of these phenotypes, strongly supports the existence of another cryptic lyso-PS receptor on mammalian macrophages (in

Please cite this article in press as: Khandelwal et al., Fatty acid chain length drives lysophosphatidylserine-dependent immunological outputs, Cell Chemical Biology (2021), https://doi.org/10.1016/j.chembiol.2021.01.008

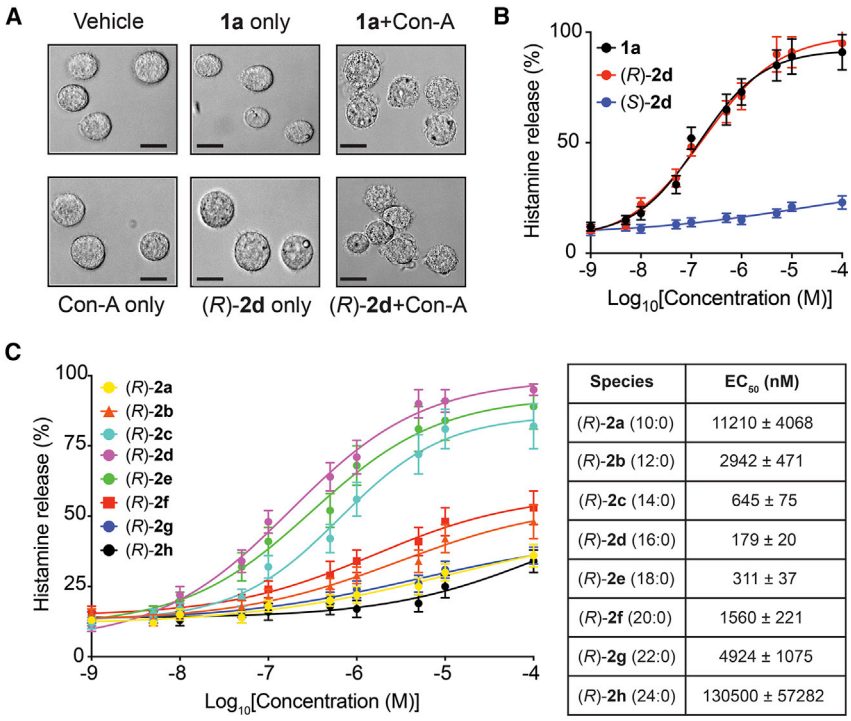

Species	EC_{50} (nM)
(*R*)-**2a** (10:0)	11210 ± 4068
(*R*)-**2b** (12:0)	2942 ± 471
(*R*)-**2c** (14:0)	645 ± 75
(*R*)-**2d** (16:0)	179 ± 20
(*R*)-**2e** (18:0)	311 ± 37
(*R*)-**2f** (20:0)	1560 ± 221
(*R*)-**2g** (22:0)	4924 ± 1075
(*R*)-**2h** (24:0)	130500 ± 57282

Figure 5. LC lyso-PSs robustly cause histamine release from primary mast cells

(A) Representative microscopy image showing degranulation of PCMCs after **1a** (C16:0 lyso-PS) or (*R*)-**2d** (C16:0) treatment (both 1 μM, 30 min, 37°C) in the presence of concanavalin A (Con-A). Scale bars, 100 μm.

(B) Histamine release profile from PCMCs treated with **1a** (C16:0 lyso-PS), (*R*)-**2d** (C16:0), or (*S*)-**2d** (C16:0) (1 nM to 10 mM, 30 min, 37°C, n = 3/data point).

(C) Dose-response and EC_{50} values for histamine release from PCMCs following treatment with the different (*R*)-Me-lyso-PSs (1 nM to 10 mM, 30 min, 37°C, n = 3/data point).

addition to TLR2) (Figure 4E). We speculate, based on aforementioned phenotypes, that this as yet unknown receptor is likely an unannotated GPCR (as putative lyso-PS GPCRs [Inoue et al., 2012] are absent in macrophages [Figures S3A and S3B]) that prefers LC lyso-PSs (particularly C18:0) as ligands to produce its downstream biological effects (Figure 4E).

LC lyso-PSs robustly induce mast cell degranulation

The release of histamine during mast cell degranulation is an extensively investigated lyso-PS-mediated immunological response (Sugo et al., 2006; Iwashita et al., 2009; Shanbhag et al., 2020), and yet contribution of individual lyso-PSs to this phenotype remain poorly understood. To address this, we generated peritoneal-derived cultured mast cells (PCMCs) (Meurer et al., 2016), and confirmed their ability to degranulate in the presence of **1a** (C16:0 lyso-PS) or the corresponding (*R*)-Me-lyso-PS, (*R*)-**2d** (C16:0) in the presence of concanavalin A (Con-A) (Figure 5A) (Iwashita et al., 2009; Sugo et al., 2006). Con-A is a well-characterized metalloprotein lectin of interest to immunologists, as it specifically binds mannosyl and/or glucosyl units of surface receptors of immune cells, and in doing so stabilizes receptor conformations that, in the context of PCMCs, facilitate lyso-PS-dependent histamine release (Lawson et al., 1978; Sullivan et al., 1975). Having shown their ability to degranulate, we quantitatively measured the histamine release from PCMCs using an established LC-MS method (Chimalakonda et al., 2015) (Figure S7). We found that the half-maximal effective concentration (EC_{50}) toward inducing histamine release during degranulation in PCMCs for **1a** (C16:0 lyso-PS, EC_{50} = 140 ± 22 nM) and (*R*)-**2d** (C16:0, EC_{50} = 179 ± 20 nM) were comparable, while the unnatural (*S*)-**2d** (C16:0, EC_{50} > 10 μM) failed to produce this phenotype (Figure 5B), suggesting that the putative receptor on PCMCs (likely GPR34 [Iwashita et al., 2009; Sugo et al., 2006; Ikubo et al., 2015], Figure S3A) is stereoselective in lyso-PS recognition. Next, we performed exhaustive dose-response studies with the (*R*)-Me-lyso-PS library and found that (*R*)-**2d** (C16:0, EC_{50} = 179 ± 20 nM) most potently induced histamine release during PCMC degranulation, with other LC (*R*)-Me-lyso-PSs (*R*)-**2e** (C18:0, EC_{50} = 311 ± 37 nM) and (*R*)-**2c** (C14:0, EC_{50} = 645 ± 75 nM) following suit (Figure 5C). This SAR study showed that medium-chain (<C12) or VLC (≥C20) (*R*)-Me-lyso-PSs failed to induce significant PCMC degranulation (EC_{50} > 2.5 μM) (Figure 5C), suggesting that besides the headgroup, the recognition of lipid tail is another major factor contributing to histamine release from mast cells during degranulation. In this SAR study, we found that the pharmacological Me-lyso-PS treatments had no effect on cell viability.

ABHD12 is the major lyso-PS lipase in primary mast cells

ABHD12 is a major lyso-PS lipase in different immune cells (Ogasawara et al., 2018; Kamat et al., 2015), but its biochemical function in primary mast cells remains unknown. Western blot analysis (Figure 6A) and diminished lyso-PS lipase activity (Figure 6B) confirmed the loss of ABHD12 in PCMCs derived from ABHD12-null mice. We also found that ABHD12-null PCMCs secreted significantly more lyso-PS (~2-fold more **1a** [C16:0] and **1b** [C18:0]) compared with WT PCMCs (Figure 6C). Given the diminished lyso-PS lipase activity, we postulated that **1a** (C16:0 lyso-PS) treatment would cause ABHD12-null PCMCs to degranulate at a lower dose of **1a**, and thereby release histamine more efficiently than WT PCMCs. Indeed, ABHD12-null PCMCs (EC_{50} = 47 ± 17 nM) released histamine more effectively than WT PCMCs (EC_{50} = 135 ± 32 nM) upon similar **1a** (C16:0 lyso-PS) treatment (Figure 6D). Finally, we measured serum histamine concentrations following intravenous (*R*)-**2d** (C16:0) injection in WT or ABHD12 knockout mice and found that ABHD12-null mice displayed heightened circulating histamine concentrations (~3-fold) compared with WT mice (Figure 6E). These results together confirm ABHD12's role as a major lyso-PS lipase in primary mast cells, where by regulating serum lyso-PS levels (Figure 6E) it controls systemic histamine release (Figure 6E).

Please cite this article in press as: Khandelwal et al., Fatty acid chain length drives lysophosphatidylserine-dependent immunological outputs, Cell Chemical Biology (2021), https://doi.org/10.1016/j.chembiol.2021.01.008

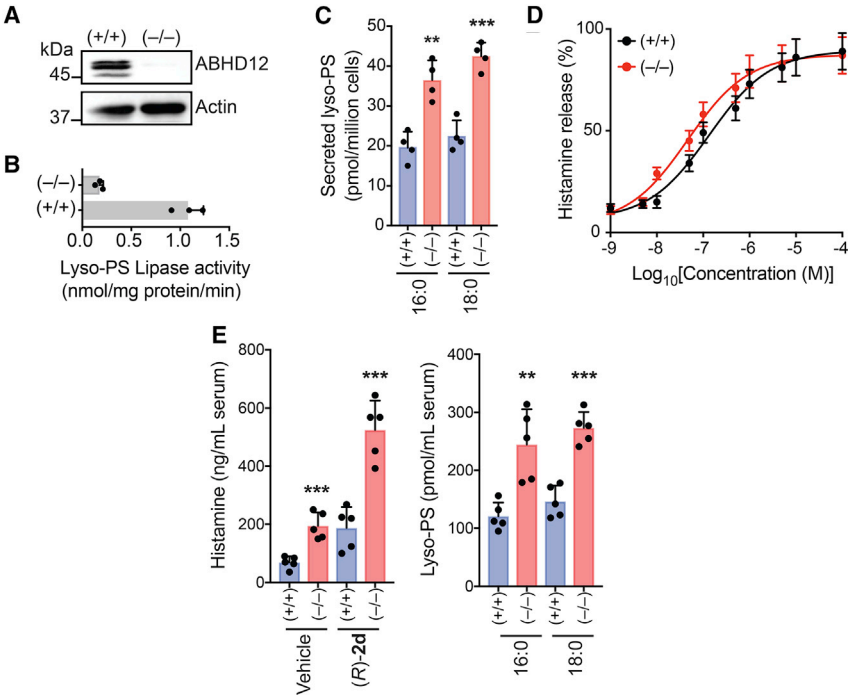

Figure 6. ABHD12 controls concentrations of LC lyso-PSs in primary mast cells, and thereby serum histamine levels

(A and B) (A) Representative western blot and (B) lyso-PS lipase activity assay (100 μM **1a** [C16:0 lyso-PS], 30 min, 37°C, n = 3/group), showing the loss of ABHD12 in PCMCs derived from ABHD12 knockout (–/–) mice.

(C) Concentrations of lyso-PS secreted from cultured PCMCs derived from WT (+/+) or ABHD12 knockout (–/–) mice, showing significantly increased **1a** (C16:0 lyso-PS) and **1b** (C18:0 lyso-PS) secretion from ABHD12-null PCMCs (n = 4/group).

(D) Histamine release profiles from PCMCs derived from WT (+/+) or ABHD12 knockout (–/–) mice treated with **1a** (C16:0 lyso-PS) (1 nM to 10 mM, 30 min, 37°C, n = 3/data point).

(E) Left: serum histamine levels in (+/+) or (–/–) mice following intravenous injections with vehicle (PBS) or (*R*)-**2d** (C16:0) (1 mg/kg, 2 h), showing increased serum histamine concentrations in the (–/–) mice compared with (+/+) controls for both treatments (n = 5/group). Interestingly, systemic administration of (*R*)-**2d** (C16:0) in (+/+) mice produces significantly more circulating serum histamine compared with the vehicle group, showing that (*R*)-**2d** (C16:0) by itself can induce histamine release from mast cells in *in vivo* settings. Right: serum lyso-PS concentrations in (+/+) or (–/–) mice, showing increased concentrations of circulating **1a** (C16:0 lyso-PS) and **1b** (C18:0 lyso-PS) in (–/–) mice, corroborating the increased serum histamine levels seen in these mice (n = 5/group). All data are presented as mean ± SD from at least n independent experiments. **p < 0.01, ***p < 0.001 versus (+/+) group by Student's two-tailed unpaired parametric t test.

DISCUSSION

Signaling lipids are potent hormone-like biological molecules that regulate several important physiological processes in mammals, and their deregulation often has detrimental consequences that eventually manifest as disease in humans. Given their direct link to human diseases, the lyso-PSs have been recently emerged as yet another important class of signaling lipids (Shanbhag et al., 2020). However, unlike the established signaling lipids (e.g., 2-AG, AEA, S1P), *in vivo* lyso-PSs exist esterified with different lipid tails ranging from medium-chain (C10–C14) to LC (C16–C20) to VLC (>C20) fatty acids (Kamat et al., 2015; Blankman et al., 2013; Singh et al., 2020). Given the vast diversity in their *in vivo* content, it remains unclear as to which of these lyso-PSs have signaling functions and how they influence, regulate, and/or modulate different immunological processes. The lack of detailed SAR studies for these immunological phenotypes for lyso-PSs stems largely from the limited commercial availability and reported synthetic strategies toward making them, especially the medium-chain and VLC variants.

In this paper, we report the synthesis of Me-lyso-PSs having (*R*)- or (*S*)-stereochemistry at the *sn*-2 position of the glycerol backbone with varying lipid tails ranging from medium-chain to LC to VLC (Figure 1 and Data S1). Since the synthesis of lyso-PSs has proved challenging, and that of VLC lyso-PSs has not been reported to the best of our knowledge, our synthetic strategy allows the performance of rigorous SAR studies in diverse assays to delineate the specific function of the lipid tail in modulating a phenotype regulated by lyso-PSs. In all our biochemical and immunological assays, we find that (*R*)-Me-lyso-PSs serve as excellent bioequivalent surrogates for the canonical (*R*)-lyso-PSs, while the corresponding (*S*)-Me-lyso-PSs are biologically inactive. Since VLC lyso-PSs have never been tested against ABHD12, despite their accumulation in the brains of ABHD12-null mice (Blankman et al., 2013; Singh et al., 2020), here, by assaying the Me-lyso-PS library, we show conclusively that the ABHD12-catalyzed lyso-PS lipase reaction is stereoselective and prefers VLC lyso-PSs as substrates (Figure 1). Furthermore, we show through biochemical assays that the (*R*)-Me-lyso-PSs are acted upon by cellular carboxylesterases and converted to the corresponding canonical (*R*)-lyso-PSs, and that therefore, biologically, the (*R*)-Me-lyso-PSs function as prodrug-like surrogates for lyso-PSs in primary macrophages and mast cells (Figure 2).

Next, we wanted to understand the distinct role played by the lipid tail of individual lyso-PSs in the activation of macrophages and mast cell degranulation, as these immunological processes have been extensively studied and reported to be regulated by lyso-PSs (Shanbhag et al., 2020). In mammalian macrophages, we find that VLC Me-lyso-PSs produce the highest secretion of pro-inflammatory cytokines and that these pro-inflammatory responses are higher in ABHD12-null macrophages (Figure 2), given their diminished lyso-PS lipase activity (Kamat et al., 2015). Next, using pharmacological tools and genetic models, we show conclusively that VLC Me-lyso-PSs (but not LC lyso-PSs) orchestrate robust pro-inflammatory responses via a TLR2-dependent pathway to cause neuroinflammation (Figure 3). That VLC lyso-PSs signal through TLR2 and cause neuroinflammation (Figures 3 and S4) raises an intriguing possibility, corroborating a recent report (Ogasawara et al., 2018) that the

Please cite this article in press as: Khandelwal et al., Fatty acid chain length drives lysophosphatidylserine-dependent immunological outputs, Cell Chemical Biology (2021), https://doi.org/10.1016/j.chembiol.2021.01.008

human neurological disease PHARC may itself be an autoimmune disease. Furthermore, we find that mammalian macrophages produce increased intracellular cAMP, cytosolic Ca^{2+} flux, and heightened ERK phosphorylation in response to LC lyso-PS treatments (particularly C18:0 lyso-PS) (Figure 4) via a TLR2-independent pathway (Figures S5 and S6), and we speculate that there is another cryptic receptor, likely a GPCR, that prefers LC lyso-PSs (particularly C18:0 lyso-PS) as ligands to produce these biological activities (Figure 4). We also show that LC lyso-PSs (especially C16:0 lyso-PS), but not medium-chain or VLC lyso-PSs, efficiently cause the release of histamine from mast cells during degranulation, suggesting that the putative lyso-PS receptor on mast cells (possibly GPR34 [Sugo et al., 2006]) prefers LC lyso-PSs (particularly C16:0 lyso-PS) as ligands to drive this immunological process (Figure 5). Finally, we report that ABHD12 is the major lyso-PS lipase in primary mast cells, where it controls the secreted lyso-PS levels, and its deletion in mice results in elevated levels of serum histamine and lyso-PS (Figure 6).

Projecting ahead, we propose that the functional antagonism of TLR2 might provide an excellent therapeutic paradigm in treating PHARC. This premise can be tested genetically by generating and characterizing ABHD12-TLR2 dual-knockout mice, and pharmacologically by discovering much needed *in vivo* active TLR2 functional antagonists. In addition, the annotation of ABHD12 as a major lyso-PS lipase in primary mast cells provides yet another avenue in understanding the immunomodulatory properties and the functional crosstalk of lyso-PSs between different immune cells particularly in the context of allergies and autoimmune conditions (Kelkar et al., 2019; Ogasawara et al., 2018). Finally, we would like to note that a major shortcoming of our study is the inability of our synthetic strategy in making Me-lyso-PSs with unsaturated fatty acid chains. Therefore, the development of such a synthetic methodology would enable making Me-lyso-PSs with unsaturated fatty acid chains and could also be leveraged to generate lyso-PS probes with suitable recently reported biorthogonal handles (Niphakis et al., 2015). Such bifunctional lyso-PS probes in tandem with advanced MS-based chemoproteomics platforms (Niphakis et al., 2015; Parker et al., 2017) will greatly facilitate the identification of hitherto unknown lyso-PS protein ligands and/or receptors, and this emerging knowledge will certainly expand our biological understanding of this underexplored immunomodulatory lipid class.

SIGNIFICANCE

Lysophospholipids are potent hormone-like biological mediators that regulate many important physiological processes in mammals. Recently, the lysophosphatidylserines (lyso-PSs) have emerged as yet another class of signaling lysophospholipids, with potent bioactivities in the central nervous and immune system in mammals, and deregulation in their metabolism has been linked to neurological and autoimmune disorders in humans. However, challenges in making lyso-PSs synthetically, and limited commercial sources for this lipid class, have greatly hampered any exhaustive structure-activity relationship (SAR) studies toward mechanistically understanding the role that lyso-PSs play in different physiological processes. Here, we report a synthetic strategy toward making methyl esters of lyso-PSs (Me-lyso-PSs) with varying lipid tails, which serve as excellent prodrug-like biological surrogates for lyso-PSs, and focus on elucidating the role that the lipid tail of this lysophospholipid plays in regulating various immunological processes. Specifically, we study the lyso-PS-mediated activation of macrophages and mast cell degranulation processes, and show through detailed SAR studies that the lipid tail has profound effects on the phenotypical outputs of these important immunological processes. Our findings thus illuminate a physiological balance between long-chain and very-long-chain lyso-PSs, intricately regulated by the lyso-PS lipase ABHD12, and that disrupting this fine-tuned homeostasis results in immunological outputs that have detrimental pathological consequences in humans.

STAR★METHODS

Detailed methods are provided in the online version of this paper and include the following:

- KEY RESOURCES TABLE
- RESOURCE AVAILABILITY
  - Lead contact
  - Materials availability
  - Data and code availability
- EXPERIMENTAL MODEL AND SUBJECT DETAILS
  - Mice
  - Mammalian cell lines
- METHOD DETAILS
  - Reagents
  - Lyso-PS lipase substrate assays
  - Mammalian cells lipid treatments
  - Western blot analysis
  - ELISA assays
  - RT-PCR
  - Immunohistochemical analysis
  - Histamine estimation from mast cells
  - Lyso-PS measurements
  - Synthesis and compound characterization
- QUANTIFICATION AND STATISTICAL ANALYSIS

SUPPLEMENTAL INFORMATION

Supplemental information can be found online at https://doi.org/10.1016/j.chembiol.2021.01.008.

ACKNOWLEDGMENTS

This work was supported by a DBT/Wellcome Trust India Alliance Fellowship (grant number IA/I/15/2/502058) awarded to S.S.K., a Department of Science and Technology (DST) Fund for Improvement of S&T Infrastructure (grant number SR/FST/LSII-043/2016) to the IISER Pune Biology Department, and a J.C. Bose National Fellowship from the Science & Engineering Research Board (SERB) (grant number SB/S2/JCB-025/2016) awarded to K.N.B. N.K. acknowledges a SERB postdoctoral fellowship, and M.S. acknowledges a graduate student fellowship from the Council of Scientific and Industrial Research. Benjamin F. Cravatt of The Scripps Research Institute is thanked for providing the ABHD12 knockout mice used in this study. The National Facility for Gene Function in Health and Disease (NFGFHD) at IISER Pune (supported by a grant from the Department of Biotechnology, Govt. of India; BT/INF/22/SP17358/2016) and

Please cite this article in press as: Khandelwal et al., Fatty acid chain length drives lysophosphatidylserine-dependent immunological outputs, Cell Chemical Biology (2021), https://doi.org/10.1016/j.chembiol.2021.01.008

Central Animal Facility at IISc Bangalore are thanked for maintaining and providing mice for this study. Sagar Tarate and Dhanashree Kelkar are thanked for technical assistance. Vineeta Bal, Satyajit Rath, Girish Deshpande, Girish Ratnaparkhi, and Nishad Matange are thanked for reading and providing critical inputs to the manuscript.

AUTHOR CONTRIBUTIONS

N.K., S.S., T.S., and A.J. performed all the biochemical studies. M.S. and A.M. synthesized and characterized all the compounds; A.M. and H.C. supervised the synthesis. K.N.B. provided the TLR2 knockout mice for this study. S.S.K. conceived the project, acquired funding, analyzed the data and wrote the paper with input from all authors.

DECLARATION OF INTERESTS

The authors declare no competing interests.

Received: August 31, 2020
Revised: November 30, 2020
Accepted: January 6, 2021
Published: February 10, 2021

REFERENCES

Barnes, M.J., Li, C.M., Xu, Y., An, J., Huang, Y., and Cyster, J.G. (2015). The lysophosphatidylserine receptor GPR174 constrains regulatory T cell development and function. J. Exp. Med. *212*, 1011–1020.

Benjamini, Y., Krieger, A.M., and Yekutieli, D. (2006). Adaptive linear step-up procedures that control the false discovery rate. Biometrika *93*, 491–507.

Blankman, J.L., and Cravatt, B.F. (2013). Chemical probes of endocannabinoid metabolism. Pharmacol. Rev. *65*, 849–871.

Blankman, J.L., Long, J.Z., Trauger, S.A., Siuzdak, G., and Cravatt, B.F. (2013). ABHD12 controls brain lysophosphatidylserine pathways that are deregulated in a murine model of the neurodegenerative disease PHARC. Proc. Natl. Acad. Sci. U S A *110*, 1500–1505.

Blankman, J.L., Simon, G.M., and Cravatt, B.F. (2007). A comprehensive profile of brain enzymes that hydrolyze the endocannabinoid 2-arachidonoylglycerol. Chem. Biol. *14*, 1347–1356.

Chimalakonda, K.C., Pang, E., Weaver, J.L., Howard, K.E., Patel, V., and Boyne, M.T. (2015). Development and validation of a liquid-chromatography tandem mass spectrometry method to determine in vitro and in vivo histamine release. J. Pharm. Biomed. Anal. *102*, 494–499.

Chu, X., Shen, M., Xie, F., Miao, X.J., Shou, W.H., Liu, L., Yang, P.P., Bai, Y.N., Zhang, K.Y., Yang, L., et al. (2013). An X chromosome-wide association analysis identifies variants in GPR174 as a risk factor for Graves' disease. J. Med. Genet. *50*, 479–485.

Contos, J.J.A., Ishii, I., and Chun, J. (2000). Lysophosphatidic acid receptors. Mol. Pharm. *58*, 1188–1196.

Dennis, E.A. (2016). Lipidomics in disease and drug discovery. Faseb J. *30*, https://doi.org/10.1096/fasebj.30.1_supplement.114.3.

Dennis, E.A., and Norris, P.C. (2015). Eicosanoid storm in infection and inflammation. Nat. Rev. Immunol. *15*, 511–523.

Fahy, E., Cotter, D., Sud, M., and Subramaniam, S. (2011). Lipid classification, structures and tools. Biochim. Biophys. Acta *1811*, 637–647.

Fahy, E., Subramaniam, S., Brown, H.A., Glass, C.K., Merrill, A.H., Jr., Murphy, R.C., Raetz, C.R., Russell, D.W., Seyama, Y., Shaw, W., et al. (2005). A comprehensive classification system for lipids. J. Lipid Res. *46*, 839–861.

Fiskerstrand, T., H'mida-Ben Brahim, D., Johansson, S., M'zahem, A., Haukanes, B.I., Drouot, N., Zimmermann, J., Cole, A.J., Vedeler, C., Bredrup, C., et al. (2010). Mutations in ABHD12 cause the neurodegenerative disease PHARC: an inborn error of endocannabinoid metabolism. Am. J. Hum. Genet. *87*, 410–417.

Fiskerstrand, T., Knappskog, P., Majewski, J., Wanders, R.J., Boman, H., and Bindoff, L.A. (2009). A novel Refsum-like disorder that maps to chromosome 20. Neurology *72*, 20–27.

Fowler, C.J., Holt, S., Nilsson, O., Jonsson, K.O., Tiger, G., and Jacobsson, S.O. (2005). The endocannabinoid signaling system: pharmacological and therapeutic aspects. Pharmacol. Biochem. Behav. *81*, 248–262.

Frasch, S.C., and Bratton, D.L. (2012). Emerging roles for lysophosphatidylserine in resolution of inflammation. Prog. Lipid Res. *51*, 199–207.

Gardell, S.E., Dubin, A.E., and Chun, J. (2006). Emerging medicinal roles for lysophospholipid signaling. Trends Mol. Med. *12*, 65–75.

Gonzalez-Cabrera, P.J., Brown, S., Studer, S.M., and Rosen, H. (2014). S1P signaling: new therapies and opportunities. F1000prime Rep. *6*, 109.

Holla, S., Prakhar, P., Singh, V., Karnam, A., Mukherjee, T., Mahadik, K., Parikh, P., Singh, A., Rajmani, R.S., Ramachandra, S.G., and Balaji, K.N. (2016). MUSASHI-mediated expression of JMJD3, a H3K27me3 demethylase, is involved in foamy macrophage generation during mycobacterial infection. PLoS Pathog. *12*, e1005814.

Hosono, H., Aoki, J., Nagai, Y., Bandoh, K., Ishida, M., Taguchi, R., Arai, H., and Inoue, K. (2001). Phosphatidylserine-specific phospholipase A1 stimulates histamine release from rat peritoneal mast cells through production of 2-acyl-1-lysophosphatidylserine. J. Biol. Chem. *276*, 29664–29670.

Ikubo, M., Inoue, A., Nakamura, S., Jung, S.J., Sayama, M., Otani, Y., Uwamizu, A., Suzuki, K., Kishi, T., Shuto, A., et al. (2015). Structure-activity relationships of lysophosphatidylserine analogs as agonists of G-protein-coupled receptors GPR34, P2Y10, and GPR174. J. Med. Chem. *58*, 4204–4219.

Inoue, A., Ishiguro, J., Kitamura, H., Arima, N., Okutani, M., Shuto, A., Higashiyama, S., Ohwada, T., Arai, H., Makide, K., and Aoki, J. (2012). TGFalpha shedding assay: an accurate and versatile method for detecting GPCR activation. Nat. Methods *9*, 1021–1029.

Ishii, I., Fukushima, N., Ye, X., and Chun, J. (2004). Lysophospholipid receptors: signaling and biology. Annu. Rev. Biochem. *73*, 321–354.

Iwashita, M., Makide, K., Nonomura, T., Misumi, Y., Otani, Y., Ishida, M., Taguchi, R., Tsujimoto, M., Aoki, J., Arai, H., and Ohwada, T. (2009). Synthesis and evaluation of lysophosphatidylserine analogues as inducers of mast cell degranulation. Potent activities of lysophosphatidylthreonine and its 2-deoxy derivative. J. Med. Chem. *52*, 5837–5863.

Joshi, A., Shaikh, M., Singh, S., Rajendran, A., Mhetre, A., and Kamat, S.S. (2018). Biochemical characterization of the PHARC-associated serine hydrolase ABHD12 reveals its preference for very-long-chain lipids. J. Biol. Chem. *293*, 16953–16963.

Kamat, S.S., Camara, K., Parsons, W.H., Chen, D.H., Dix, M.M., Bird, T.D., Howell, A.R., and Cravatt, B.F. (2015). Immunomodulatory lysophosphatidylserines are regulated by ABHD16A and ABHD12 interplay. Nat. Chem. Biol. *11*, 164–171.

Kelkar, D.S., Ravikumar, G., Mehendale, N., Singh, S., Joshi, A., Sharma, A.K., Mhetre, A., Rajendran, A., Chakrapani, H., and Kamat, S.S. (2019). A chemical-genetic screen identifies ABHD12 as an oxidized-phosphatidylserine lipase. Nat. Chem. Biol. *15*, 169–178.

Kimura, I., Moritani, Y., and Tanizaki, Y. (1973). Basophils in bronchial asthma with reference to reagin-type allergy. Clin. Allergy *3*, 195–202.

Lawson, D., Fewtrell, C., and Raff, M.C. (1978). Localized mast cell degranulation induced by concanavalin A-Sepharose beads. Implications for the Ca2+ hypothesis of stimulus-secretion coupling. J. Cell Biol. *79*, 394–400.

Lee, S.Y., Lee, H.Y., Kim, S.D., Jo, S.H., Shim, J.W., Lee, H.J., Yun, J., and Bae, Y.S. (2008). Lysophosphatidylserine stimulates chemotactic migration in U87 human glioma cells. Biochem. Biophys. Res. Commun. *374*, 147–151.

Liang, Q.L., Wu, Q.A., Jiang, J.H., Duan, J.A., Wang, C., Smith, M.D., Lu, H., Wang, Q., Nagarkatti, P., and Fan, D.P. (2011). Characterization of Sparstolonin B, a Chinese herb-derived compound, as a selective toll-like receptor antagonist with potent anti-inflammatory properties. J. Biol. Chem. *286*, 26470–26479.

Liang, Q.L., Yu, F., Cui, X.D., Duan, J.A., Wu, Q.N., Nagarkatti, P., and Fan, D.P. (2013). Sparstolonin B suppresses lipopolysaccharide-induced inflammation in human umbilical vein endothelial cells. Arch. Pharmacal Res. *36*, 890–896.

Please cite this article in press as: Khandelwal et al., Fatty acid chain length drives lysophosphatidylserine-dependent immunological outputs, Cell Chemical Biology (2021), https://doi.org/10.1016/j.chembiol.2021.01.008

Lloret, S., and Moreno, J.J. (1995). Ca^{2+} influx, phosphoinositide hydrolysis, and histamine release induced by lysophosphatidylserine in mast cells. J. Cell Physiol. *165*, 89–95.

Mallik, S., Prasad, R., Bhattacharya, A., and Sen, P. (2018). Synthesis of phosphatidylserine and its stereoisomers: their role in activation of blood coagulation. ACS Med. Chem. Lett. *9*, 434–439.

Meurer, S.K., Ness, M., Weiskirchen, S., Kim, P., Tag, C.G., Kauffmann, M., Huber, M., and Weiskirchen, R. (2016). Isolation of mature (peritoneum-derived) mast cells and immature (bone marrow-derived) mast cell precursors from mice. PLoS One *11*, e0158104.

Napier, C., Mitchell, A.L., Gan, E., Wilson, I., and Pearce, S.H.S. (2015). Role of the X-linked gene GPR174 in autoimmune Addison's disease. J. Clin. Endocrinol. Metab. *100*, E187–E190.

Navia-Paldanius, D., Savinainen, J.R., and Laitinen, J.T. (2012). Biochemical and pharmacological characterization of human alpha/beta-hydrolase domain containing 6 (ABHD6) and 12 (ABHD12). J. Lipid Res. *53*, 2413–2424.

Niphakis, M.J., Lum, K.M., Cognetta, A.B., 3rd, Correia, B.E., Ichu, T.A., Olucha, J., Brown, S.J., Kundu, S., Piscitelli, F., Rosen, H., and Cravatt, B.F. (2015). A global map of lipid-binding proteins and their ligandability in cells. Cell *161*, 1668–1680.

Ogasawara, D., Ichu, T.A., Vartabedian, V.F., Benthuysen, J., Jing, H., Reed, A., Ulanovskaya, O.A., Hulce, J.J., Roberts, A., Brown, S., et al. (2018). Selective blockade of the lyso-PS lipase ABHD12 stimulates immune responses in vivo. Nat. Chem. Biol. *14*, 1099–1108.

Park, K.S., Lee, H.Y., Kim, M.K., Shin, E.H., and Bae, Y.S. (2005). Lysophosphatidylserine stimulates leukemic cells but not normal leukocytes. Biochem. Biophys. Res. Commun. *333*, 353–358.

Parker, C.G., Galmozzi, A., Wang, Y., Correia, B.E., Sasaki, K., Joslyn, C.M., Kim, A.S., Cavallaro, C.L., Lawrence, R.M., Johnson, S.R., et al. (2017). Ligand and target discovery by fragment-based screening in human cells. Cell *168*, 527–541 e29.

Pathak, D., Mehendale, N., Singh, S., Mallik, R., and Kamat, S.S. (2018). Lipidomics suggests a new role for ceramide synthase in phagocytosis. ACS Chem. Biol. *13*, 2280–2287.

Raetz, C.R., and Whitfield, C. (2002). Lipopolysaccharide endotoxins. Annu. Rev. Biochem. *71*, 635–700.

Rajendran, A., Vaidya, K., Mendoza, J., Bridwell-Rabb, J., and Kamat, S.S. (2020). Functional annotation of ABHD14B, an orphan serine hydrolase enzyme. Biochemistry *59*, 183–196.

Rosen, H., Stevens, R.C., Hanson, M., Roberts, E., and Oldstone, M.B. (2013). Sphingosine-1-phosphate and its receptors: structure, signaling, and influence. Annu. Rev. Biochem. *82*, 637–662.

Rueden, C.T., Schindelin, J., Hiner, M.C., Dezonia, B.E., Walter, A.E., Arena, E.T., and Eliceiri, K.W. (2017). ImageJ2: ImageJ for the next generation of scientific image data. BMC Bioinformatics *18*, 529.

Schindelin, J., Rueden, C.T., Hiner, M.C., and Eliceiri, K.W. (2015). The ImageJ ecosystem: an open platform for biomedical image analysis. Mol. Reprod. Dev. *82*, 518–529.

Shanbhag, K., Mhetre, A., Khandelwal, N., and Kamat, S.S. (2020). The lysophosphatidylserines—an emerging class of signalling lysophospholipids. J. Membr. Biol. *253*, 381–397.

Singh, S., Joshi, A., and Kamat, S.S. (2020). Mapping the neuroanatomy of ABHD16A, ABHD12, and lysophosphatidylserines provides new insights into the pathophysiology of the human neurological disorder PHARC. Biochemistry *59*, 2299–2311.

Sugita, K., Yamamura, C., Tabata, K., and Fujita, N. (2013). Expression of orphan G-protein coupled receptor GPR174 in CHO cells induced morphological changes and proliferation delay via increasing intracellular cAMP. Biochem. Biophys. Res. Commun. *430*, 190–195.

Sugo, T., Tachimoto, H., Chikatsu, T., Murakami, Y., Kikukawa, Y., Sato, S., Kikuchi, K., Nagi, T., Harada, M., Ogi, K., et al. (2006). Identification of a lysophosphatidylserine receptor on mast cells. Biochem. Biophys. Res. Commun. *341*, 1078–1087.

Sullivan, T.J., Greene, W.C., and Parker, C.W. (1975). Concanavalin A-induced histamine release from normal rat mast cells. J. Immunol. *115*, 278–282.

Szymanski, K., Miskiewicz, P., Pirko, K., Jurecka-Lubieniecka, B., Kula, D., Hasse-Lazar, K., Krajewski, P., Bednarczuk, T., and Ploski, R. (2014). rs3827440, a nonsynonymous single nucleotide polymorphism within GPR174 gene in X chromosome, is associated with Graves' disease in Polish Caucasian population. Tissue Antigens *83*, 41–44.

Tracey, T.J., Steyn, F.J., Wolvetang, E.J., and Ngo, S.T. (2018). Neuronal lipid metabolism: multiple pathways driving functional outcomes in health and disease. Front. Mol. Neurosci. *11*, 10.

Van Der Kleij, D., Latz, E., Brouwers, J.F., Kruize, Y.C., Schmitz, M., Kurt-Jones, E.A., Espevik, T., De Jong, E.C., Kapsenberg, M.L., Golenbock, D.T., et al. (2002). A novel host-parasite lipid cross-talk. Schistosomal lyso-phosphatidylserine activates toll-like receptor 2 and affects immune polarization. J. Biol. Chem. *277*, 48122–48129.

Vance, J.E. (2015). Phospholipid synthesis and transport in mammalian cells. Traffic *16*, 1–18.

Wu, C., Jin, X., Tsueng, G., Afrasiabi, C., and Su, A.I. (2016). BioGPS: building your own mash-up of gene annotations and expression profiles. Nucleic Acids Res. *44*, D313–D316.

Wymann, M.P., and Schneiter, R. (2008). Lipid signalling in disease. Nat. Rev. Mol. Cell Biol. *9*, 162–176.

Yanagida, K., and Valentine, W.J. (2020). Druggable lysophospholipid signaling pathways. Adv. Exp. Med. Biol. *1274*, 137–176.

Please cite this article in press as: Khandelwal et al., Fatty acid chain length drives lysophosphatidylserine-dependent immunological outputs, Cell Chemical Biology (2021), https://doi.org/10.1016/j.chembiol.2021.01.008

STAR★METHODS

KEY RESOURCES TABLE

REAGENT or RESOURCE	SOURCE	IDENTIFIER
Antibodies		
Rabbit, anti-phospho-p44/42 MAPK (ERK1/2) (20G11)	Cell Signaling Technology	Clone: monoclonal, catalog# 4376, RRID: AB_331772
Rabbit, anti-p44/42 MAPK (ERK1/2) (137F5)	Cell Signaling Technology	Clone: monoclonal, catalog# 4695, RRID: AB_390779
Rabbit, anti-GAPDH (EPR16891)	Abcam	Clone: monoclonal, catalog# ab181602, RRID: AB_2630358
Rabbit, anti-ABHD12 (EPR13683-72) (produced recombinantly, animal free)	Abcam	Clone: monoclonal, catalog# ab182011, RRID: Not available
Rabbit, anti-Iba1 (EPR16588)	Abcam	Clone: monoclonal, catalog# ab178846, RRID: AB_2636859
Rabbit, anti-beta actin	Cloud-Clone Corp.	Clone: polyclonal, catalog# CAB340Hu01, RRID: Not available
Rabbit, anti-TLR2	Novus Biologicals	Clone: polyclonal, catalog# NB100-56720, RRID: AB_838993
Goat, anti-rabbit IgG (H + L) secondary antibody, HRP conjugated	Thermo Fisher Scientific	Clone: polyclonal, catalog# 31,460, RRID: AB_228341
Horse, anti-rabbit IgG (H + L) secondary antibody, Biotinylated	Vector Laboratories	Clone: polyclonal, catalog# BP-1100, RRID: Not available
Critical commercial assays		
Mouse TNF-alpha DuoSet	R&D Systems	Catalog# DY410
Mouse IL-6 DuoSet	R&D Systems	Catalog# DY406
Human TNF-alpha DuoSet	R&D Systems	Catalog# DY210
Human IL-6 DuoSet	R&D Systems	Catalog# DY206
cAMP assay kit (competitive ELISA)	Abcam	Catalog# ab65355
Flou-8 calcium assay kit – medium removal	Abcam	Catalog# ab112128
ERK1 (pT202/pY204) + ERK2 (pT185/pY187) + total ERK1/2 ELISA kit	Abcam	Catalog# ab126445
Chemicals, peptides and recombinant proteins		
C16:0 Lyso-PS	Avanti Polar Lipids	Catalog# 858142
C18:0 Lyso-PS	Avanti Polar Lipids	Catalog# 858144
C18:1 Lyso-PS	Avanti Polar Lipids	Catalog# 858143
C17:1 Lyso-PS	Avanti Polar Lipids	Catalog# 858141
C18:0 Lyso-PA	Avanti Polar Lipids	Catalog# 857128
C18:0 Lyso-PG	Avanti Polar Lipids	Catalog# 858124
C18:0 Lyso-PC	Avanti Polar Lipids	Catalog# 855775
cis-10-Heptadecenoic acid (C17:1 FFA)	Sigma-Aldrich (Merck)	Catalog# H8896
Stearic acid	Sigma-Aldrich (Merck)	Catalog# S4751
Thioglycollate medium	Sigma-Aldrich (Merck)	Catalog# T9032
Lipopolysaccharide	Sigma-Aldrich (Merck)	Catalog# L3024
Mouse interleukin-3	Sigma-Aldrich (Merck)	Catalog# I4144
Mouse stem cell factor	Sigma-Aldrich (Merck)	Catalog# S9915
Sparstolonin B (SpaB)	Sigma-Aldrich (Merck)	Catalog# SML1767
Carboxylesterase from porcine liver	Sigma-Aldrich (Merck)	Catalog# 46,058
Histamine	Sigma-Aldrich (Merck)	Catalog# H7125
Concanavalin A (Con-A)	Sigma-Aldrich (Merck)	Catalog# C0412
Polyethylenimine hydrochloride (PEI MAX®)	Polysciences	Catalog# 24,765

(*Continued on next page*)

Please cite this article in press as: Khandelwal et al., Fatty acid chain length drives lysophosphatidylserine-dependent immunological outputs, Cell Chemical Biology (2021), https://doi.org/10.1016/j.chembiol.2021.01.008

Continued

REAGENT or RESOURCE	SOURCE	IDENTIFIER
Experimental models: organisms/strains		
Mouse: C57BL/6J	The Jackson Laboratory	RRID: IMSR_JAX:000664
Mouse: ABHD12 null	Scripps Research	N/A
Mouse: TLR2 null	The Jackson Laboratory	RRID: IMSR_JAX:004650
Experimental models: cell lines		
HEK293T cells	ATCC	RRID: CVCL_0063
THP-1 cells	ATCC	RRID: CVCL_0006
Oligonucleotides		
Primers for RT-PCR, see Table S1	This paper	N/A
Software and algorithms		
Prism 7 (version 7.0e)	GraphPad	https://www.graphpad.com/scientific-software/prism/
ImageJ v1.52u	NIH	https://imagej.nih.gov/ij/
SciexOS (version 1.4.0.18067)	Sciex	https://sciex.com/products/software/sciex-os-software-x120805
Other		
Lipidomics data (mass spec)	This paper	Available from lead contact upon reasonable request

RESOURCE AVAILABILITY

Lead contact

Further information and materials request should be directed to and will be fulfilled only by the Lead Contact, Siddhesh S. Kamat (siddhesh@iiserpune.ac.in).

Materials availability

Any compounds, or reagents described/generated in this study, are available with the Lead Contact upon request with a completed Materials Transfer Agreement.

Data and code availability

All the data that supports the findings of this study are available in the paper (and its associated Supplemental information) or are available from the Lead Contact on reasonable request. No unique codes were generated in this study.

EXPERIMENTAL MODEL AND SUBJECT DETAILS

Mice

All mouse studies and experiments described in this paper have received formal approval from the Indian Institute of Science Education and Research, Pune – Institutional Animal Ethics Committee (IISER-P IAEC) (application nos: IISER_Pune IAEC/2016_02/01, and IISER_Pune IAEC/2019_2/07) constituted as per the guidelines and norms provided by the Committee for the Purpose of Control and Supervision of Experiments in Animals (CPCSEA), Government of India. All experimental mice were housed in the National Facility for Gene Function in Health and Disease (NFGFHD), IISER Pune, and were studied between 2 – 6 months of age. All mice had *ab libitum* access to food and water. Thioglycollate elicited primary peritoneal macrophages (PPMs) (Singh et al., 2020; Kelkar et al., 2019) and peritoneal-derived cultured mast cells (PCMCs) (Meurer et al., 2016) were generated from mice 10 – 12 weeks of age, harvested from mice and cultured using established protocols. For all mouse experiments, equal number of male and female mice were used, and age/sex matched littermates were used as controls. All strains of mice used in this study as reported in the Key resources table.

Mammalian cell lines

HEK293T (RRID: CVCL_0063, female) and THP-1 (RRID: CVCL_0006, male) cells were purchased from the ATCC, and cultured in RPMI1640 medium supplemented with 10% (v/v) FBS and antibiotics (1% (v/v) penicillin-streptomycin (MP Biomedicals)) at 37°C with 5% (v/v) CO_2. Cell staining with 4′,6-diamidino-2-phenylindole (DAPI) was routinely performed to ensure that all cell lines were devoid of any mycoplasma contamination. All cell lines were grown to ~80% confluency, and all live cells were estimated on a TC20 automated cell counter using trypan blue reagent as per manufacturer's protocol (Bio-Rad).

Please cite this article in press as: Khandelwal et al., Fatty acid chain length drives lysophosphatidylserine-dependent immunological outputs, Cell Chemical Biology (2021), https://doi.org/10.1016/j.chembiol.2021.01.008

METHOD DETAILS

Reagents

Unless otherwise mentioned, all the following materials used in the experiments described in this paper were purchased from the commercial source mentioned in the parenthesis: chemicals, buffers and reagents (Sigma-Aldrich), commercial lipids and lipid standards (Avanti Polar Lipids), primary and secondary antibodies (Abcam), and tissue culture media and Fetal Bovine Serum (FBS) (HiMedia).

Lyso-PS lipase substrate assays

Wild type (WT) human ABHD12 (hABHD12) or the catalytically inactive active site mutant S246A hABHD12 were transiently transfected in HEK293T cells using a polyethylenimine-based (PEI MAX®) transfection methodology (Joshi et al., 2018; Kamat et al., 2015) along with mock (empty plasmid) controls, and the membrane lysates from these were prepared as reported earlier (Kelkar et al., 2019; Joshi et al., 2018). Briefly, HEK293T cells overexpressing either WT ABHD12 or S246A ABHD12 or "mock" control (empty plasmid) were harvested by scraping 48 hours post-transfection, washed (3x) with cold sterile Dulbecco's phosphate buffer saline (DPBS) without calcium and magnesium (pH 7.2) (HiMedia), re-suspended 1 mL DPBS, and lysed by sonication. The cell debris (pellet) was discarded after centrifugation at 200g for 5 min at 4°C, and the resulting lysate (supernatant, ~ 900 μL) was centrifuged at 100,000g for 45 min at 4°C. The supernatant from this step was also discarded, and the pellet (membrane proteome) was washed (3x) with cold sterile DPBS, and re-suspended to uniformity by pipetting in 500 μL of cold sterile DPBS. The protein concentration was estimated using BCA Protein assay kit (Pierce), and the expression of hABHD12 in this cell membrane lysate was confirmed by western blot analysis (Joshi et al., 2018). The brain membrane lysates from wild type and ABHD12 knockout mice were also prepared using a protocol reported earlier (Joshi et al., 2018; Singh et al., 2020). Briefly, the mice were anaesthetized using isoflurane, and euthanized by cervical dislocation. The mouse brains were harvested, and washed (3x) using DBPS. Following this, a half brain was suspended in 500 μL of cold sterile DBPS, and homogenized by a tissue homogenizer (Bullet Blender 24, Next Advance) using 1 scoop of glass beads (0.5 mm diameter, Next Advance) for 3 min at 4°C at an instrument speed setting of 8. To this brain homogenate, cold sterile DPBS (500 μL) was added, mixed to uniformity by pipetting, centrifuged at 1000g for 5 min at 4°C to precipitate the tissue debris. The supernatant lysate (~700 μL) from this step was collected, and centrifuged at 100,000g for 45 min at 4°C. The resulting supernatant was discarded and the pellet (membrane proteome) was washed with cold sterile DPBS (3x), re-suspended in 1 mL of cold sterile DPBS by pipetting, and the final protein concentration of the brain membrane lysate was estimated using the BCA Protein assay kit (Pierce). The lyso-PS lipase assays described in this paper were performed using an established LC-MS method that measures the release of free fatty acids from lyso-PS substrates by the lipase activity of ABHD12 relative to an unnatural fatty acid internal standard (C17:1 FFA, 0.5 nmol/sample) (Joshi et al., 2018; Singh et al., 2020). All assays done using 10 μg of HEK293T membrane lysates transfected with hABHD12 or 20 μg of brain membrane lysates for 30 mins, as previous studies have shown that the lyso-PS lipase assay is linear for this protein concentration and time over a range of substrate concentrations (Joshi et al., 2018). All single concentration lipase (substrate) assays were done using 100 μM of the lipid substrate, while the enzyme kinetic studies were done over the concentration range of 0 – 400 μM for the particular lipid that was assayed.

Mammalian cells lipid treatments

Primary peritoneal macrophages (PPMs) were freshly obtained from mice using a protocol previously reported by us (Singh et al., 2020; Kelkar et al., 2019) with typical yields of (~10 x 10^6) PPMs per mouse. Briefly, PPMs were elicited by intraperitoneal injection of aged thioglycollate broth (3% w/v) and 60 hours post-injection, the PPMs were harvested by a peritoneal lavage using 10 mL cold sterile DBPS. Post-harvest, the cells were pelleted by centrifugation at 1400g for 5 mins, and re-suspended in 5 mL of RBC lysis buffer for 10 mins at 4°C. After removal of the RBC lysis buffer by centrifugation at 1400g for 5 mins at 4°C, the PPMs were re-suspended in 5 mL of RPMI 1640 medium supplemented with 10% (v/v) FBS and antibiotics (1% (v/v) penicillin-streptomycin (MP Biomedicals)) at 37°C with 5% (v/v) CO_2, following which, live PPMs were estimated on a TC20 automated cell counter using trypan blue reagent as per manufacturer's protocol (Bio-Rad) and plated at the required cell density as per the desired assay condition. PPMs were allowed to adhere to the plates for 2 h at 37°C and 5% (v/v) CO_2, following which, the media was replaced to that required for the desired assay. Equal number of male and female mice were used for the generation of PPMs. For the pro-inflammatory cytokine measurements, macrophages (1 x 10^6 PPMs or 0.5 x 10^6 THP-1 cells) were plated in 6-well plates (Eppendorf) in 2 mL of RPMI1640 media without any supplementation, and treated with vehicle (DMSO) or lipids [commercial lyso-PSs or (*R*)-Me-lyso-PSs or (*S*)-Me-lyso-PSs or free fatty acids, or other C18:0 lysophospholipids (lyso-PA, lyso-PG and lyso-PC)] or LPS (positive assay control) all at 1 μM final concentration for 4 hours at 37°C. Following this treatment, the media (1.5 mL) was collected and stored at –80°C till the analysis was completed. The pro-inflammatory cytokines (TNF-α and IL-6) were quantitatively measured using standard single analyte ELISA assays as per manufacturer's instructions (R&D Systems). For the cellular cyclic adenosine 5′-monophosphate (cAMP), cytosolic calcium (Ca^{2+}) and ERK phosphorylation measurements, macrophages (4 x 10^6 PPMs or 2 x 10^6 THP-1 cells) were plated in 6-well plates (Eppendorf) in 3 mL of RPMI1640 media without any supplementation, and treated with vehicle (DMSO) or lipids [commercial lyso-PSs or (*R*)-Me-lyso-PSs or (*S*)-Me-lyso-PSs or free fatty acids, or other C18:0 lysophospholipids (lyso-PA, lyso-PG and lyso-PC)] or LPS (positive assay control) all at 1 μM final concentration for 10 mins at 37°C. Following this treatment, the assay plates were centrifuged at 1400g for 5 min to pellet the live cells, and separate the media. The media was removed by pipetting, following which, the cells were washed with sterile cold DPBS (x 3 times) at 4°C, and lysed by sonication in 500 μL cold sterile

Please cite this article in press as: Khandelwal et al., Fatty acid chain length drives lysophosphatidylserine-dependent immunological outputs, Cell Chemical Biology (2021), https://doi.org/10.1016/j.chembiol.2021.01.008

DPBS at 4°C. The cell lysates were deproteinized by passing them through a 3000 (3-kDa) molecular weight filter, and the flow through was eventually used to estimate the cellular levels of cAMP and free cytosolic Ca^{2+}. For phosphorylated ERK measurements, total cell lysates without the deproteinization step were used. The changes (increase) in cellular cAMP, free cytosolic Ca^{2+} and ERK phosphorylation in response to the aforementioned treatments were quantitatively estimated using standard competitive ELISA based colorimetric (cAMP, ERK phosphorylation) and fluorometric (free cytosolic Ca^{2+}) assays as per manufacturer's instructions (Abcam). All pharmacological TLR2 antagonism studies (Liang et al., 2011, 2013) described in this paper, were done at 10 μM final concentration of SpaB for 4 hours at 37°C. The number of live cells were estimated at the end of every experiment or assay using the trypan blue reagent on a TC20 automated cell counter by as per manufacturer's protocol (Bio-Rad), to ensure that the pharmacological treatments were not affecting cell viability.

Western blot analysis

Cell or tissue lysates were prepared as described earlier (Joshi et al., 2018), the protein concentrations from them were estimated using the Pierce BCA Protein Assay kit (Thermo Fisher Scientific), and the western blot analysis was done using previously reported protocols (Rajendran et al., 2020; Joshi et al., 2018). Briefly, 50 μg protein lysate was resolved on a 12% SDS-PAGE gel and transferred onto a PVDF membrane (GE Healthcare) (60 mA, 12 h, 4°C). Post-transfer, the membrane was blocked with 5% (w/v) skimmed milk in 1X phosphate buffered saline containing 0.1% (w/v) Tween-20 (PBST) (blocking buffer) for 1 h at room temperature (20 – 25°C), washed with PBST (x 3 times) and subsequently probed with the primary antibody (dilution 1:1000) in blocking buffer for 12 – 14 h at 4°C. Following this, the membrane was washed with PBST (x 3 times), and incubated with a horse-radish peroxidase (HRP) conjugated anti-rabbit IgG (H + L) (goat, Thermo Fisher Scientific, 31,460, 1:10,000) secondary antibody for 1 h at room temperature (20 – 25°C). Finally, the membrane was washed with PBST (x 3 times), and the signal was visualized with SuperSignal West Pico Chemiluminescent substrate (Thermo Fisher Scientific) on a Syngene G-Box Chemi-XRQ gel documentation system. For the phosphoprotein immunoblotting, the cells and tissues were lysed in buffer containing phosphatase inhibitors (1 mM sodium orthovanadate, 1 mM sodium pyrophosphate, 5 mM sodium fluoride) to maintain intact protein phosphorylation at serine, threonine and/or tyrosine protein residues. A complete list of all the primary antibodies used in this study can be found in the Key resources table.

ELISA assays

All quantitative pro-inflammatory cytokine measurements (TNF-α, IL-6) were done using single analyte ELISA assays from R&D Systems as per manufacturer's instructions. For measuring intracellular cAMP, cytosolic free Ca^{2+} and phosphorylated ERK, ELISA kits were purchased from Abcam, and the assays were performed as per manufacturer's instructions. A complete list of all the ELISA kits used in this study can be found in the Key resources table.

RT-PCR

The total RNA was isolated from mouse PPM using the RiboZol™ RNA extraction reagent (Amresco), and the first strand cDNA was synthesized from the isolated total RNA using the ThermoScript™ RT-PCR System (Invitrogen) as per manufacturer's protocol. The primers and the fragment size for the gene products analyzed in this study are listed in Table S1, and the gel for the RT-PCR experiment is presented in Figure S3B.

Immunohistochemical analysis

The immunohistochemical analysis were done using a protocol recently published by us with minor modifications (Singh et al., 2020). Briefly, mice were deeply anaesthetized using isoflurane and perfused first with cold phosphate buffer saline (PBS), and then with 4% (w/v) paraformaldehyde (PFA) in PBS. Brains were dissected and post-fixed in 4% (w/v) PFA in PBS overnight at 4°C and then transferred into 30% (w/v) sucrose in PBS until brains sank to bottom of the tubes (~3 days). Coronal 25 μm cerebellar sections were cut on a freezing microtome (Leica CM1950), maintained at – 30°C and 1 out of every 6 sections was collected for assessing microglial activation. Endogenous peroxidases were inactivated with 3% (v/v) hydrogen peroxide in PBS for 15 min. Thereafter the sections were washed twice with 1% bovine serum albumin (BSA) (HiMedia) in PBS, and permeabilized with 0.1% (w/v) Triton-X 100 and 0.5% (w/v) BSA in PBS at room temperature (20 – 25°C) for 45 mins. The sections were then incubated with primary monoclonal anti-Iba1 antibody [rabbit, Abcam, Cat: ab178846, 1:1000] in 1% (w/v) BSA in PBS overnight at 4°C. Following overnight incubation, the sections were washed three times with 0.5% (w/v) BSA in PBS and incubated with secondary antibody, biotinylated anti-rabbit [horse, Vector labs, BP-1100, 1:500] in 0.5% (w/v) BSA in PBS for 1 h at room temperature (20 – 25°C). Following this treatment, the sections were washed twice in 0.5% (w/v) BSA in PBS, incubated with ABC Elite Vectastatin (Vector labs, Cat: PK-6100) for 1 h at room temperature (20 – 25°C) and subsequently washed twice with excess PBS. Finally, the sections were stained with Immpact DAB (Vector labs, Cat: SK-4105) for 3 min in the dark, transferred to excess PBS and mounted in VectaMount (Vector labs, Cat: H-5000) after drying. Activated microglial cells (area >200 μm^2) in matching cerebellar sections were quantified using the ImageJ software (NIH) (Rueden et al., 2017; Schindelin et al., 2015) as per previously reported protocols (Blankman et al., 2013; Singh et al., 2020).

Histamine estimation from mast cells

The PCMCs were isolated from the peritoneal cavity of mice (10 -12 weeks of age) and cultured using a previously reported protocol (Meurer et al., 2016) with typical yields of ~ (1 x 10^6) PCMCs per mouse. Briefly, cells from the mice peritoneal cavity were harvested by lavage, using 10 mL cold sterile DBPS, and re-suspended in RPMI 1640 medium supplemented with 10% (v/v) FBS, antibiotics

Please cite this article in press as: Khandelwal et al., Fatty acid chain length drives lysophosphatidylserine-dependent immunological outputs, Cell Chemical Biology (2021), https://doi.org/10.1016/j.chembiol.2021.01.008

(1% (v/v) penicillin-streptomycin (MP Biomedicals)), 50 μM β-mercaptoethanol, 10 ng/mL recombinant mouse interleukin-3, and 30 ng/mL mouse stem cell factor at 37°C with 5% (v/v) CO_2. The cells were plated initially at a density of 0.5 x 10^6 cells/mL, and 48 hours post-plating, the non-adherent cells were removed by replacing the spent media with fresh media containing all the aforementioned components. The adherent cells were allowed to grow and differentiate into PCMCs over the next 10 – 15 days with fresh media supplementation (spent media was not discarded) on the 6th day, and the purity of the PCMCs was assessed by Kimura staining (Kimura et al., 1973). Live PCMCs were estimated on a TC20 automated cell counter using trypan blue reagent as per manufacturer's protocol (Bio-Rad) and used at the required cell density as per the desired assay condition. To assess the extent of lyso-PS induced degranulation of PCMCs, histamine release from these cells was measured using an established LC-MS method (Chimalakonda et al., 2015), which we validated using an authentic histamine standard (Figure S7). Towards this, PCMCs were first pelleted (1400g for 5 min) and subsequently re-suspended in Hank's Balanced Salt Solution (HBSS) containing 1% (w/v) heat inactivated FBS at a concentration of 5 x 10^6 cells/mL. All assays were performed in a 96 well plates with "V" bottoms (Tarsons) to a final volume of 100 μL at 37°C with 5% (v/v) CO_2. The vehicle (DMSO) or lipids (commercial lyso-PSs or (*R*)-Me-lyso-PSs or (*S*)-Me-lyso-PSs; ranging from 1 nM – 100 μM concentration in the assay) were added to individual wells with or without Con-A (1 mg/mL final assay concentration) to make volume to 90 μL in HBSS. To this, 10 μL of the PCMC cell stock (5 x 10^6 cells/mL) pre-incubated at 37°C with 5% (v/v) CO_2 was added such that each assay well finally contained 5 x 10^3 cells, and the assay allowed to proceed for 30 mins at 37°C with 5% (v/v) CO_2. At this point, to quench the assay, the cells were pelleted by centrifugation (1200g for 5 mins), and 50 μL of the media was collected for estimation of secreted histamine levels. To this 50 μL of media, 150 μL of LC-MS grade acetonitrile (Sigma-Aldrich) was added, the mixture was vortexed and stored at – 80°C till the histamine estimations were performed by LC-MS. The pellet cells were re-suspended in the remaining 50 μL media by vigorous vortexing and lysed by sonication in a water bath at 37°C. The cell lysates were then added to 150 μL of MS grade acetonitrile (Sigma-Aldrich), the mixture was vigorously vortexed and stored at – 80°C till the histamine estimations were performed. The histamine release from PCMCs was calculated in accordance to a formula reported for this LC-MS method (Chimalakonda et al., 2015). For measuring circulating serum histamine concentrations, 1 volume of mouse serum (typically 200 – 300 μL) obtained from whole blood of wild type or ABHD12 knockout mice (12 – 14 weeks of age), was mixed with 2 volumes (400 – 600 μL) MS grade acetonitrile (Sigma-Aldrich), the mixture was centrifuged at 2000g for 5 mins to pellet the protein debris, and the supernatant was collected, dried, and re-suspended in 50 μL MS grade acetonitrile (Sigma-Aldrich), and assessed thereafter by LC-MS as per a previously reported protocol (Chimalakonda et al., 2015). The quantitation for serum histamine levels, was done using a standard calibration curve for histamine (5 – 5000 ng/mL serum). All histamine measurements were done using an established LC-MS method (Chimalakonda et al., 2015) in the positive ion mode using high resolution multiple reaction monitoring (MRM-HR) analysis on a Sciex X500R quadrupole time-of flight (QTOF) mass spectrometer fitted with an Exion UHPLC system using a Kinetex 2.6 μm HILIC column with 100 Å particle size, 150 mm length and 3 mm internal diameter (Phenomenex). The MRM-HR mass spectrometry parameters for measuring histamine are: precursor ion mass (Q1, M + H^+) = 112.0869, product ion mass (Q3, M + H^+) = 95.0604, declustering potential = 100 V, entrance potential = 10 V, collision energy = 50 V, and collision exit potential = 10 V. Complete details of the sensitivity and dynamic range of the LC-MS method for histamine estimation, and the co-elution studies with a histamine standard can be found in Figure S7.

Lyso-PS measurements

The organic extractions to enrich lyso-PS lipids, and all the LC-MS based quantitative lyso-PS measurements (secreted lyso-PS concentrations from PCMCs (Figure 6C), and the serum lyso-PS levels (Figure 6E)) were performed using an established and previously reported protocols by us (Kelkar et al., 2019; Singh et al., 2020; Pathak et al., 2018). Briefly, to 1 mL of serum free spent media from PCMCs (Figure 6C) or mouse serum diluted to 1 mL using DPBS (Figure 6E), 3 mL of 2:1 (v/v) chloroform: methanol containing 1 nmol of C17:1 lyso-PS (internal standard) was added. This mixture was vortexed, and then centrifuged at 2800g for 15 mins at 4°C to separate the organic and aqueous layer. The organic layer (bottom) was collected, and the aqueous layer was acidified with 20 μL MS grade formic acid. The acidified aqueous phase was vortexed, and the volume was subsequently adjusted to 4 mL using chloroform. This mixture was vortexed, and centrifuged at 2800g for 15 mins at 4°C and organic layer (bottom) was collected. The organic layers from both the extraction steps were pooled and dried under a stream of nitrogen gas at room temperature. The dried lipid extract was re-suspended in 150 μL of 2:1 (v/v) chloroform: methanol and 20 μL of it was injected into the LC-MS for lyso-PS measurements. Area under the curve for detected lyso-PS species was normalized to area under the curve for C17:1 lyso-PS (internal standard) and absolute lyso-PS concentrations were obtained by normalized either to number of live cells (Figure 6C) or volume of serum (Figure 6E). The measurements of lyso-PS (product) formed following porcine liver carboxylesterase (0.1 U, 15 mins, 37°C) or immune cell lysate (ABHD12-null PPM or PCMC, 20 μg, 15 mins, 37°C) treatment of Me-lyso-PS (100 μg) was also done using the same reported protocols (Singh et al., 2020; Kelkar et al., 2019; Joshi et al., 2018).

Synthesis and compound characterization

Complete details of synthesis of all the compounds reported in this paper, their chemical/analytical characterization and all the spectral data associated with these compounds can be found in the Data S1 associated with this paper.

Please cite this article in press as: Khandelwal et al., Fatty acid chain length drives lysophosphatidylserine-dependent immunological outputs, Cell Chemical Biology (2021), https://doi.org/10.1016/j.chembiol.2021.01.008

CellPress

QUANTIFICATION AND STATISTICAL ANALYSIS

All bar graphs or data points represent mean of the experimental data, and the error bars represent the standard deviation from the mean, as indicated in the figure legends. *N* denotes the exact number of biological replicates per experimental group, unless stated otherwise in the figure legends. All statistical analyses were performed using the GraphPad Prism 7 (version 7.0e) software for Mac OS. The Student's two-tailed unpaired parametric *t*-test with a 95% confidence interval using a two-stage linear step up procedure of Benjamini, Krieger and Yekutieli (Benjamini et al., 2006) was used to determine the statistical significance between the different study groups in Figures 2B, 6C, and 6E, and a p value of <0.05 was considered statistical significant for all the assays reported in this study. p value annotations used in this study: *<0.05, **<0.01, and ***<0.001.